



Universiteit
Leiden
The Netherlands

Fast and efficient generation of knock-in human organoids using homology-independent CRISPR-Cas9 precision genome editing

Artegiani, B.; Hendriks, D.; Beumer, J.; Kok, R.; Zheng, X.; Joore, I.; ... ; Clevers, H.

Citation

Artegiani, B., Hendriks, D., Beumer, J., Kok, R., Zheng, X., Joore, I., ... Clevers, H. (2020). Fast and efficient generation of knock-in human organoids using homology-independent CRISPR-Cas9 precision genome editing. *Nature Cell Biology*, 22, 321-331.
doi:10.1038/s41556-020-0472-5

Version: Publisher's Version
License: [Creative Commons CC BY 4.0 license](#)
Downloaded from: <https://hdl.handle.net/1887/3181947>

Note: To cite this publication please use the final published version (if applicable).



Fast and efficient generation of knock-in human organoids using homology-independent CRISPR–Cas9 precision genome editing

Benedetta Artegiani^{1,2,7}, Delilah Hendriks^{1,7}, Joep Beumer¹, Rutger Kok³, Xuan Zheng³, Indi Joore¹, Susana Chuva de Sousa Lopes⁴, Jeroen van Zon³, Sander Tans³ and Hans Clevers^{1,2,5,6} ✉

CRISPR–Cas9 technology has revolutionized genome editing and is applicable to the organoid field. However, precise integration of exogenous DNA sequences into human organoids is lacking robust knock-in approaches. Here, we describe CRISPR–Cas9-mediated homology-independent organoid transgenesis (CRISPR–HOT), which enables efficient generation of knock-in human organoids representing different tissues. CRISPR–HOT avoids extensive cloning and outperforms homology directed repair (HDR) in achieving precise integration of exogenous DNA sequences into desired loci, without the necessity to inactivate TP53 in untransformed cells, which was previously used to increase HDR-mediated knock-in. CRISPR–HOT was used to fluorescently tag and visualize subcellular structural molecules and to generate reporter lines for rare intestinal cell types. A double reporter—in which the mitotic spindle was labelled by endogenously tagged tubulin and the cell membrane by endogenously tagged E-cadherin—uncovered modes of human hepatocyte division. Combining tubulin tagging with TP53 knock-out revealed that TP53 is involved in controlling hepatocyte ploidy and mitotic spindle fidelity. CRISPR–HOT simplifies genome editing in human organoids.

Organoids can be generated by guided differentiation of induced pluripotent stem cells and embryonic stem cells, or from cells isolated from adult tissues¹. Adult stem cell (ASC)-derived organoids are self-organizing structures that recapitulate aspects of cellular composition, three-dimensional (3D) architecture and functionality of the different epithelial tissues from which they originate, while maintaining genomic stability^{2,3}. The possibility to derive organoids from genetically modified mouse lines, especially knock-in models, has enabled the generation of engineered mouse organoids that have been used as versatile *in vitro* tools to answer various biological questions^{4–10}.

The generation of engineered human ASC-derived organoids requires that efficient strategies for *in vitro* genome editing are applied after the lines have been established. CRISPR–Cas9 technology has simplified genetic engineering considerably. To date, these approaches were largely limited to the non-homologous end joining (NHEJ)-mediated introduction of indels into the endogenous loci of organoids, leading to gene mutations^{11–14}. By harnessing the HDR pathway, a single-base substitution was introduced to correct the CFTR locus in cystic fibrosis intestinal organoids¹⁵, and a few human ASC-organoid knock-in reporter lines have been generated, but mostly in colon cancer organoids^{16–18}.

Knock-in using HDR takes advantage of a mechanism used by cells to repair double-stranded breaks (DSBs). Such breaks can be introduced at specific sites using CRISPR–Cas9. HDR is the most commonly used approach for targeted insertion, but this process is inefficient and requires cells to be in S phase^{19,20}. Furthermore, HDR requires that the donor plasmid is cloned, owing to the necessity for the presence of homology arms specific to each gene (Fig. 1a). Recent studies have shown that CRISPR-induced DSBs activate the

TP53 damage response and induce a transient cell-cycle arrest in untransformed cells²¹. Permanent or transient inactivation of TP53 increases HDR-mediated knock-in in pluripotent and hematopoietic stem cells^{22,23}. Thus, given the demand for novel methods to improve HDR efficiency, inhibition of TP53 was suggested as a potential solution to overcome the low efficiency of HDR-mediated knock-in in untransformed cells²³.

NHEJ, another key DNA repair system, is active in all cell cycle phases²⁰ and, by ligating DNA ends, does not require regions of homology (Fig. 1a). As NHEJ is generally believed to be error prone, it is not widely used for precision transgene insertion. However, it has been suggested that NHEJ can be fundamentally accurate and can religate DNA ends without errors^{24,25}. Indeed, a handful of studies have exploited NHEJ to ensure the targeted insertion of exogenous DNA into zebrafish²⁶, mouse²⁷, immortalized human cell lines^{28,29} and embryonic stem cells³⁰. Here we leverage NHEJ-mediated knock-in for use in the human organoid field—an approach named CRISPR–HOT—as a versatile, efficient and robust homology-independent method to obtain knock-in human wild-type organoids from different organs.

Results

CRISPR–HOT is a powerful strategy to efficiently generate knock-in human organoids. We first set out to test (1) the efficiency of the conventional HDR approach, (2) whether NHEJ can be used for precise genome editing and knock-in of exogenous DNA at specific genomic loci and (3) a side-by-side comparison of the two strategies. For HDR, we used donor plasmids containing a fluorescent tag (tdTomato or mNEON) flanked by 0.5 kb homology arms to C-terminally target *KRT19* or *TUBB* in human liver

¹Hubrecht Institute, KNAW (Royal Netherlands Academy of Arts and Sciences), Utrecht, the Netherlands. ²Oncode Institute, Utrecht, the Netherlands.

³AMOLF, Amsterdam, the Netherlands. ⁴Leiden University Medical Center, Anatomy and Embryology, Leiden, the Netherlands. ⁵University Medical Center Utrecht, Cancer Genomics Netherlands, Utrecht, the Netherlands. ⁶The Princess Maxima Center for Pediatric Oncology, Utrecht, the Netherlands.

⁷These authors contributed equally: Benedetta Artegiani, Delilah Hendriks. ✉e-mail: h.clevers@hubrecht.eu

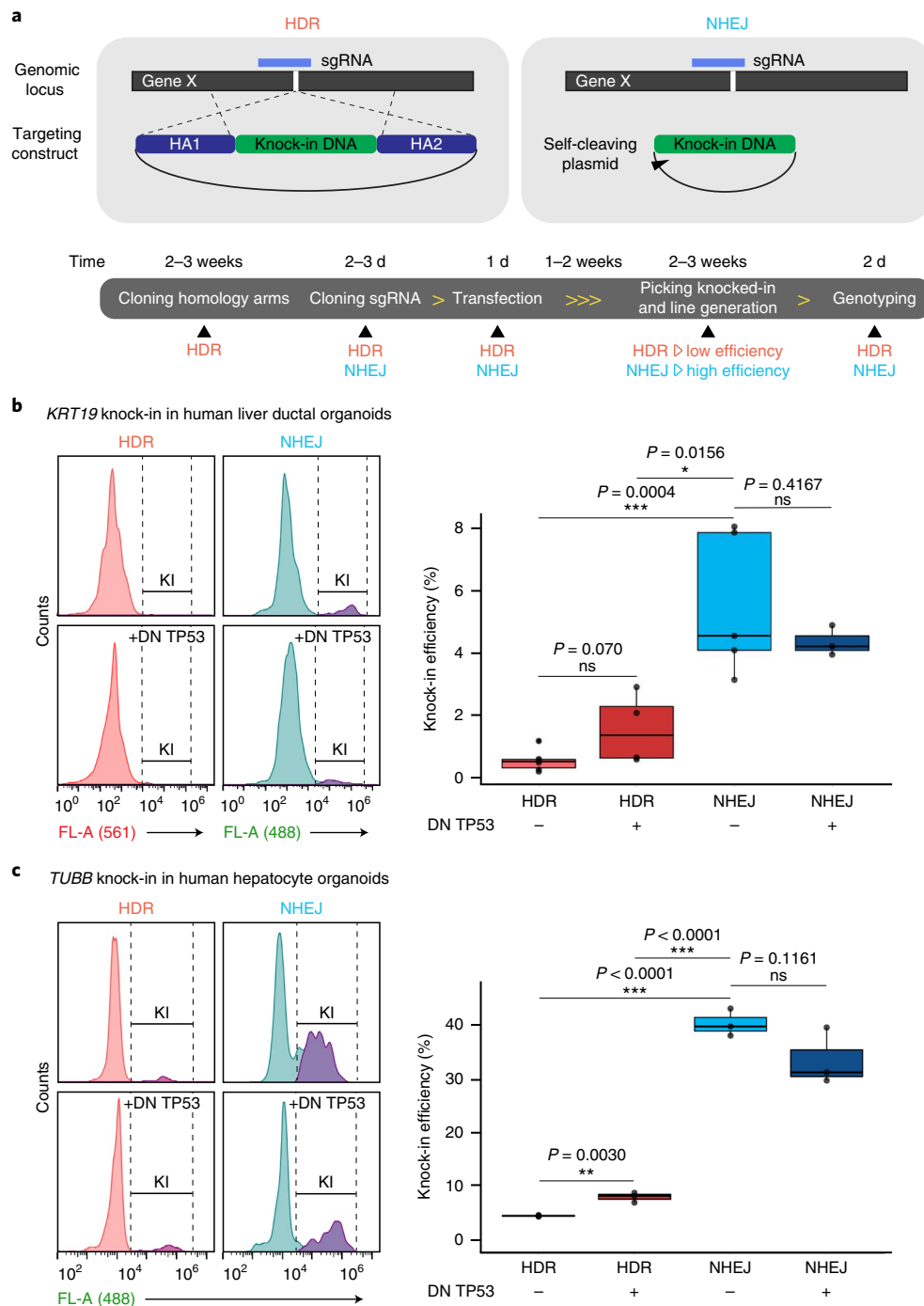


Fig. 1 | CRISPR-HOT strategy and efficiency. **a**, Principle and stepwise schematic of using HDR or NHEJ to obtain knock-in of exogenous DNA into the genomic locus of interest, and the associated timeline. The number of yellow arrowheads between the steps are scaled to time. Note that, for NHEJ, a targeting plasmid was used that is cleavable by a sgRNA at the 5' end of the knock-in tag. **b**, Flow-cytometry histograms showing the knock-in (KI) efficiency at the *KRT19* locus in transfected human liver ductal cells using HDR (red) or NHEJ (blue) with or without transient TP53 inhibition (by overexpression of a dominant negative form of TP53 (DN TP53)). Quantification of the percentage of knocked-in cells over the transfected cells in the different conditions is shown on the right. Data are derived from organoid lines from at least 3 different donors; $n=6$ for HDR–DN TP53, $n=4$ for HDR+DN TP53, $n=5$ for NHEJ–DN TP53 and $n=3$ for NHEJ+DN TP53 biological independent experiments. **c**, Comparison of the knock-in efficiency at the *TUBB* locus in transfected human hepatocytes using HDR or NHEJ with or without transient TP53 inhibition, determined using FACS analysis as described in **b**; $n=3$ biological independent experiments. For **b** and **c**, statistical analysis was performed using two-sided unpaired t-tests; * $P < 0.05$; ** $P < 0.01$; *** $P < 0.001$; ns, not significant. For the box plots in **b** and **c**, the boxes indicate the 25–75th percentiles, the centre line indicates the mean and the lines indicate the minimum and maximum values. Source data are available online.

ductal organoids and human hepatocyte organoids, respectively. For NHEJ, we utilized a universal targeting plasmid containing a fluorescent protein (mNEON) for C-terminal gene tagging

(an overview and schematic representation of all of the targeting plasmids used in this study is provided in Extended Data Fig. 1). This plasmid is cleavable due to the upstream incorporation of a

non-human sequence that can be recognized by a single guide RNA (sgRNA) and, therefore, mediates linearization of the plasmid by CRISPR–Cas9 (refs. 28,29). To promote in-frame knock-in, this non-human sequence can be targeted by three different sgRNAs (frame selectors). Each of these frame selectors mediates the cut in one of the three possible frames^{28,29}.

We tested this in two different—and difficult to transfect—human organoid systems from the two main epithelial cell types of the liver (human liver ductal cells³¹ and hepatocytes³²). All cells in liver ductal organoids abundantly express KRT19 (ref. 31). To test knock-in efficiencies at the *KRT19* locus in human liver ductal organoids, we used a transfection method that we described recently¹³. For HDR, we used the HDR targeting plasmid, a plasmid expressing Cas9 and a fluorescent marker as a transfection readout, and a plasmid expressing a sgRNA inducing a DSB directly upstream of the *KRT19* stop codon. For NHEJ, we used the universal NHEJ self-cleaving targeting plasmid, the same KRT19 sgRNA plasmid as described for HDR and the appropriate frame selector, which also expresses Cas9 and a fluorescent marker (mCherry) as a transfection readout. Five days after transfection, we observed some knocked-in cells in the HDR condition (mean \pm s.d. = $0.55 \pm 0.35\%$), as measured by fluorescence-activated cell sorting (FACS) analysis of knocked-in cells within the transfected population (transfection efficiency ranged from 0.2% to 0.7% in both HDR and NHEJ experiments). By contrast, we found that significantly more knocked-in cells appeared when testing NHEJ-mediated gene insertion (mean \pm s.d. = $5.53 \pm 2.26\%$; Fig. 1b, Extended Data Fig. 2a–c).

We next tested the knock-in efficiencies by HDR and NHEJ in human hepatocyte organoids, targeting the *TUBB* locus. For this organoid system, we adapted a different transfection method, relying on cuvette electroporation. We again observed a considerably higher efficiency of NHEJ (mean \pm s.d. = $40.23 \pm 2.54\%$) compared with HDR-mediated knock-in (mean \pm s.d. = $4.70 \pm 0.15\%$) within the transfected population (transfection efficiency ranging from 9% to 14%; Fig. 1c, Extended Data Fig. 2a,b). Outgrowing knocked-in organoids from both conditions displayed similar localization of the fluorescent signal, characteristic of TUBB expression patterns (Extended Data Fig. 2e). We named this NHEJ-mediated knock-in approach in organoids CRISPR–HOT.

Recently, transient TP53 inhibition was shown to improve the efficiency of HDR in human pluripotent stem cells²² and hematopoietic stem cells²³. We therefore performed a direct comparison between HDR and CRISPR–HOT in the presence of transient TP53 inhibition by cotransfecting a dominant negative form of TP53 (DN TP53)^{22,33}. Although the presence of DN TP53 increased HDR efficiency both in human liver ductal (absolute knock-in efficiency, mean \pm s.d. = $1.56 \pm 1.13\%$) and hepatocyte (absolute knock-in efficiency, mean \pm s.d. = $8.18 \pm 0.93\%$) organoids by twofold (Fig. 1b,c), it was still much lower than the efficiencies obtained using NHEJ (Extended Data Fig. 2d). Transient TP53 inhibition did not affect NHEJ-mediated knock-in efficiency (Fig. 1b,c). Notably, although absolute knock-in efficiencies between the two organoid systems was variable, relative fold changes between HDR, NHEJ, and the presence or absence of DN TP53 were remarkably similar (Extended Data Fig. 2d). Thus, these results demonstrate that CRISPR–HOT can mediate DNA insertion in human organoids at higher efficiency than previously used methods.

CRISPR–HOT mediates precise gene insertion. We next evaluated the frequency at which DNA integration is precise when using CRISPR–HOT. To this end, we targeted two different loci, *CDH1* and *TUBB*, in human hepatocyte organoids. After sorting transfected mCherry⁺ cells using FACS, we quantified the proportion of outgrowing mNEON⁺ and mNEON[−] organoids from these single cells. We then picked individual clonal organoids and sequenced both knocked-in mNEON⁺ organoids as well as mNEON[−]

organoids (Fig. 2a,b). When targeting *CDH1*, 33% of the organoids had precise in-frame knock-in; for *TUBB*, this proportion was 40%, levels that were comparable to our previous observation of knock-in efficiency at this locus (Fig. 2b compared with Fig. 1c), indicating that the vast majority of knocked-in cells also have the ability to grow out as organoids. Analysis of the mNEON[−] organoids revealed a small percentage of imprecise out-of-frame knock-in events due to the introduction of small indels (*CDH1*, 10%; *TUBB*, 3% of the total population), whereas the rest did not have insertions (both *CDH1* and *TUBB*, 56% of the total population; Fig. 2b).

Next, as the introduction of a Cas9-mediated DSB could generate indels in the allele that was not targeted by the knock-in event, we PCR-amplified and sequenced the DNA region around the cut site. By analysing five different loci that were targeted across two different human organoid systems (liver ductal and hepatocyte), indels were found at only two loci (*CDH1*, 12.5%; *TUBB*, 25%; Fig. 2c). Altogether these results show that it is possible to select for the desired genotype on both alleles on the basis of sequencing, and the likelihood to obtain the desired genotype is high. We next constructed a double-frame selector strategy in which the tag of interest was flanked by two frame-selector cassettes on both the 5' and 3' ends such that the reading frame of the remaining 3' end of the targeted gene can stay intact (Fig. 2d). As a proof of concept, we validated this approach by targeting *TUBB* with this double-frame plasmid in human hepatocyte organoids. We observed mNEON⁺ organoids, and the sequencing of multiple independent clonal organoids revealed precise in-frame insertions at both the 5' and 3' ends of the inserted mNEON tag, therefore leaving the *TUBB* 3' untranslated region intact (Fig. 2d). This double-frame selector strategy is an important asset that could also potentially be applied to tag genes at the N terminus. Taken together, CRISPR–HOT can mediate precise in-frame insertions with high efficiency while maintaining the second allele intact.

Generation of human liver ductal reporter organoid lines by CRISPR–HOT. We next evaluated whether we could derive clonal organoid lines from human liver ductal cells expressing endogenously tagged KRT19–mNEON. Two days after electroporation, transfected organoids were picked on the basis of transient mCherry expression from the frame-selector plasmid and dissociated into single cells to grow clonal lines¹³ (Fig. 3a). Single knocked-in mNEON⁺ organoids were picked and grown out as *KRT19::mNEON* clonal lines. Correct insertion at the *KRT19* locus was validated by sequencing (Fig. 3b,c). As expected, mNEON expression was observed in every cell in *KRT19::mNEON* organoids. Staining for ZO-1 and actin confirmed that these knock-in organoids showed robust epithelial polarization, which is typical for human liver ductal organoids (Fig. 3c). Cytoplasmic cellular distribution was also in agreement with the expected KRT19 localization by antibody co-staining (Fig. 3d).

Another keratin, KRT18, was targeted as a second locus to validate the robustness of our approach. Again, precise in-frame integration was obtained when targeting this locus (Extended Data Fig. 3a). Expression of KRT18–mNEON was confined to the cytoplasm and high-resolution imaging confirmed labelling of intermediate filaments (Fig. 3e). Together, our data show that hard-to-transfect human liver ductal organoids can be genome-edited to generate clonal knock-in reporter lines using CRISPR–HOT.

CRISPR–HOT enables labelling of rare intestinal cell types. We next tested whether CRISPR–HOT also works in other human organoid models from other organs. Human intestinal organoids can be induced to contain several differentiated cell types, mirroring the cell types present in the intestine in vivo^{34,35}. In contrast to mouse intestinal organoids, differentiation of human intestinal organoids is less efficient^{8,35}. Rare intestinal cell types, such as hormone-producing enteroendocrine cells, are therefore relatively

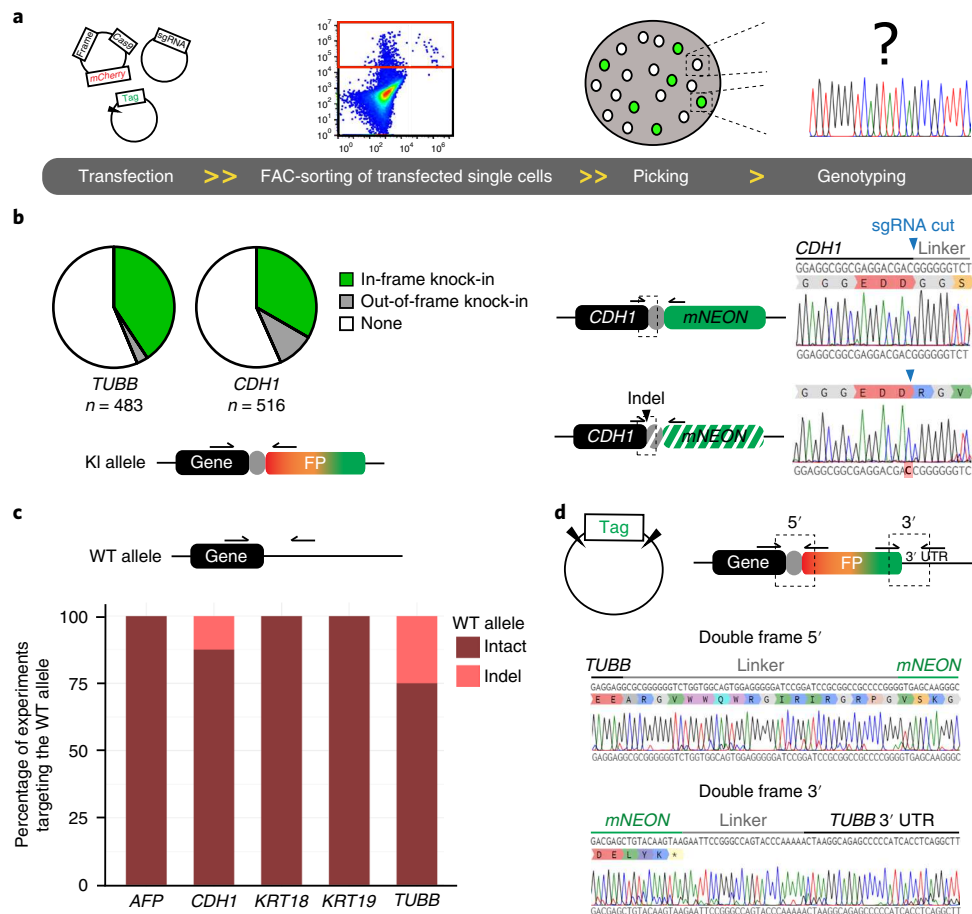


Fig. 2 | CRISPR-HOT enables precise gene knock-in. **a**, Schematic of the experimental set-up to assess the preciseness of NHEJ-mediated knock-in events. Human hepatocyte organoids were transfected with the NHEJ plasmids, single transfected cells were sorted using FACS and outgrowing clonal organoids (both mNEON⁺ and mNEON⁻) were sequenced. **b**, Sequencing of the PCR amplicons using primers spanning the region of the knock-in shows that CRISPR-HOT mediates predominantly precise in-frame knock-in at two different loci (*TUBB* and *CDH1*) in human hepatocyte organoids; *n* = 483 (*TUBB*) and *n* = 516 (*CDH1*) biologically independent samples (left). Right, representative sequencing examples of in-frame and out-of-frame knock-in events at the *CDH1* locus. FP, fluorescent protein. Dashed boxes represent the sequenced region and the highlighted base the frameshift indel. **c**, Analysis of the untargeted allele from clonal and bulk organoid lines knocked-in at five different loci. The percentage of WT alleles in different experiments for the different loci that are either carrying indels or are intact is shown; *n* = 9 independent experiments. **d**, A double-frame selector enables the targeting plasmid to be cleaved at both the 5' and 3' end of the tagging cassette. This plasmid was tested at the *TUBB* locus. Sequencing of both the 5' and 3' ends demonstrates precise knock-in of this excised tag at both ends. Sequencing examples that are representative of multiple clonal organoids are shown. The experiment was repeated twice independently with similar results. UTR, untranslated region. Source data are available online.

sparse compared with mouse intestinal organoids. However, generation of reporter lines to identify and enrich for these human cell types can help studies to understand their functions and regulation.

We tested CRISPR-HOT in human intestinal organoids by adapting a different transfection method based on cuvette electroporation of small clumps of cells³⁶ and sorting using FACS after 5–7 d (Fig. 4a). We targeted a broadly and constitutively expressed gene (*CDH1*) as well as two marker genes expressed in specific and rare cell types (*CHGA* for enteroendocrine cells and *MUC2* for goblet cells). For *CDH1*, we were able to directly pick clonal knocked-in organoids that grew out after sorting (Fig. 4a). By contrast, for *CHGA* and *MUC2*, we used a short differentiation pulse (specific to the desired cell population)^{8,37}, which could be reversed by switching the culture conditions back to expansion medium. This approach enables visualization of positive cells within one knocked-in organoid derived from one single cell that was sorted using FACS, which can be picked to establish clonal knock-in organoid lines (Fig. 4a). Accordingly, when we targeted the *CDH1* locus, we could already identify knocked-in mNEON⁺ cells within the transfected cells (transfection efficiency

ranging from 1.6–2.6%) during FACS analysis (Fig. 4b). By contrast, as expected, we did not observe any mNEON⁺ cells when targeting the *CHGA* or *MUC2* locus (Fig. 4b) as fluorescence can be visualized only after induction of gene expression related to the differentiation into the respective cell type.

The human intestinal organoids expressing endogenously tagged E-cadherin mNEON (E-CAD-mNEON) (mean \pm s.d. = $28.6 \pm 0.1\%$ knock-in efficiency) could be picked and readily grown into *CDH1::mNEON* clonal lines. E-CAD-mNEON showed typical membrane expression in all of the KRT20⁺ enterocytes (Fig. 4c). For *CHGA*, we picked single knock-in organoids (mean \pm s.d. = $20.2 \pm 5.0\%$ knock-in efficiency) on the basis of a short differentiation pulse using previously described enteroendocrine cell enrichment medium⁸, and established *CHGA::mNEON* clonal organoid lines. After expansion and subsequent differentiation, these organoids contained rare enteroendocrine (*CHGA*-mNEON⁺) cells with fluorescently marked vesicles, i.e., secretory granules (Fig. 4d). These cells stained for CHGA protein, while a proportion also produced the neurotransmitter serotonin (Fig. 4d). For *MUC2*, we used a similar approach, but

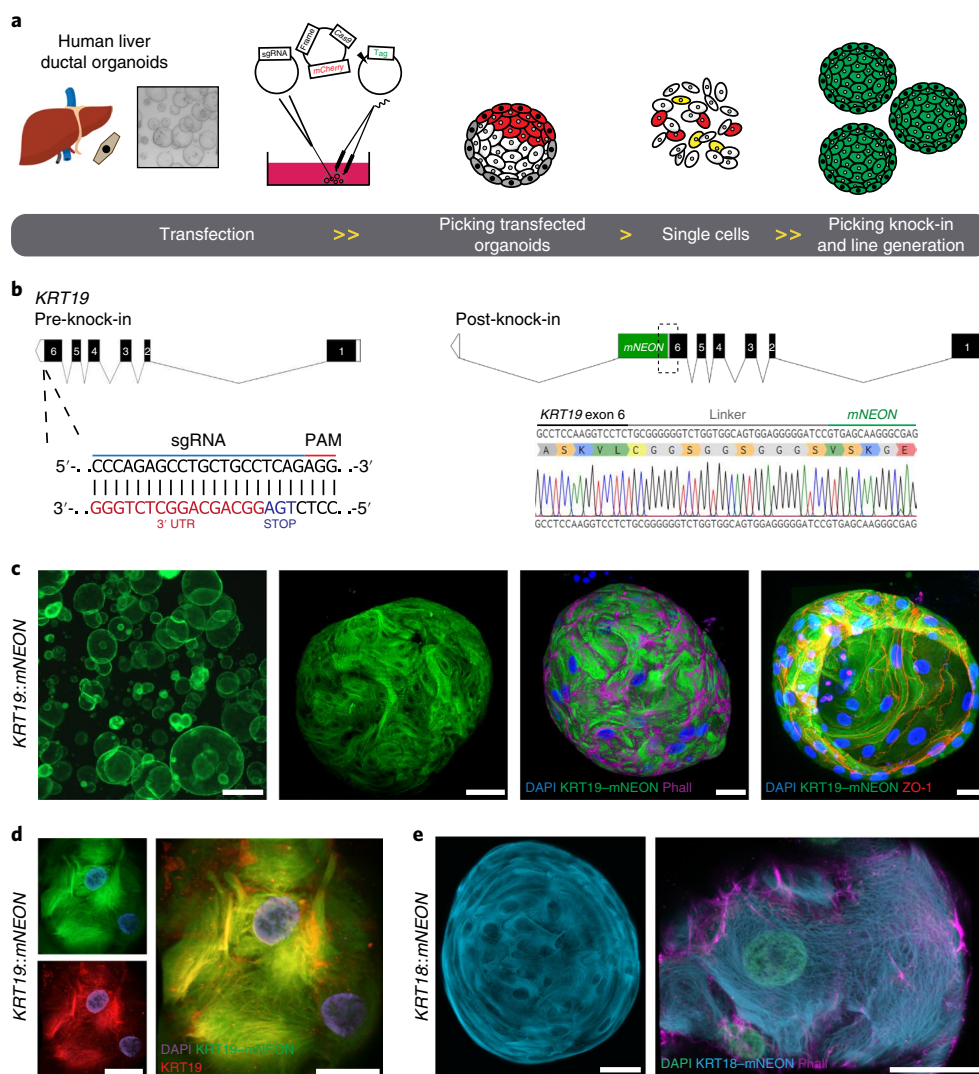


Fig. 3 | Generation of human liver ductal reporter organoid lines using CRISPR-HOT. a, Transfection and knock-in generation strategy for human liver ductal organoids. DNA is microinjected into the lumen of the organoids grown in a droplet of reduced growth-factor basement-membrane extract (BME^R) using a glass capillary, after which the BME^R droplet is electroporated using a tweezer electrode. Organoids with transfected cells are picked on the basis of transient mCherry expression from the frame selector plasmid and made into single cells. In-frame knocked-in mNEON⁺ organoids growing from these single cells are subsequently picked to establish clonal reporter lines. **b**, The strategy and sgRNA, including its PAM sequence, used to tag the human *KRT19* locus. Schematic overview of the *KRT19* locus before and after knock-in. A representative sequencing result confirms in-frame knock-in of mNEON at the *KRT19* locus. **c**, Representative fluorescence image of a clonal *KRT19::mNEON* culture at low and high magnification (left). Right, whole-mount image of a *KRT19::mNEON* organoid stained with phalloidin and ZO-1. **d**, Co-staining of *KRT19::mNEON* with an anti-*KRT19* antibody demonstrates overlapping signals. **e**, Representative fluorescence image of a clonal *KRT18::mNEON* culture (left). Right, high-magnification imaging of a *KRT18::mNEON* organoid. The endogenous *KRT18*-mNEON fusion enables the visualization of the intermediate filament structures; the actin cytoskeleton is visualized using phalloidin. A schematic of the *KRT18* locus before and after knock-in, and representative sequencing results of the *KRT18::mNEON* line are provided in Extended Data Figs. 3a and 8a. For **b–e**, all of the experiments were repeated three times independently with similar results. Scale bars, for **c**, 400 μ m, 50 μ m, 20 μ m and 20 μ m (left to right); **d**, 20 μ m (left) and 10 μ m (right); and **e**, 20 μ m (left) and 10 μ m (right).

in this case used a differentiation pulse based on the addition of the Notch inhibitor DAPT³⁷. Clonal organoid lines could be established and—after differentiation—contained cells expressing MUC2-mNEON showing the typical morphology of goblet cells (Fig. 4e). For all of the targeted loci, the derived lines showed precise in-frame knock-in, as confirmed by sequencing (Extended Data Fig. 3b,c), altogether validating the robustness of CRISPR-HOT.

Generation of clonal human hepatocyte reporter organoid lines using CRISPR-HOT. We next evaluated whether we could establish clonal lines from CRISPR-HOT knocked-in human hepatocytes. Organoids were first dissociated into single cells and then transfected

using cuvette electroporation (Fig. 5a). We picked the knocked-in organoids that grew after transfection on the basis of fluorescence and established clonal lines. First, we successfully targeted *AFP*, a gene that is exclusively expressed in hepatocyte organoids by almost all cells³², and generated clonal *AFP::mNEON* lines (Fig. 5b, Extended Data Fig. 3d). These organoids showed typical hepatocyte morphological features, such as the formation of bile canaliculi networks, as visualized by MRP2 staining (Fig. 5b). *AFP* in these organoids had the same pattern of expression visualized by antibody staining, yet the *AFP*-mNEON signal appeared to have higher signal resolution (Fig. 5b).

Similar to the intestinal organoids, we were able to derive clonal *CDH1::mNEON* hepatocyte lines (Fig. 5c). The presence

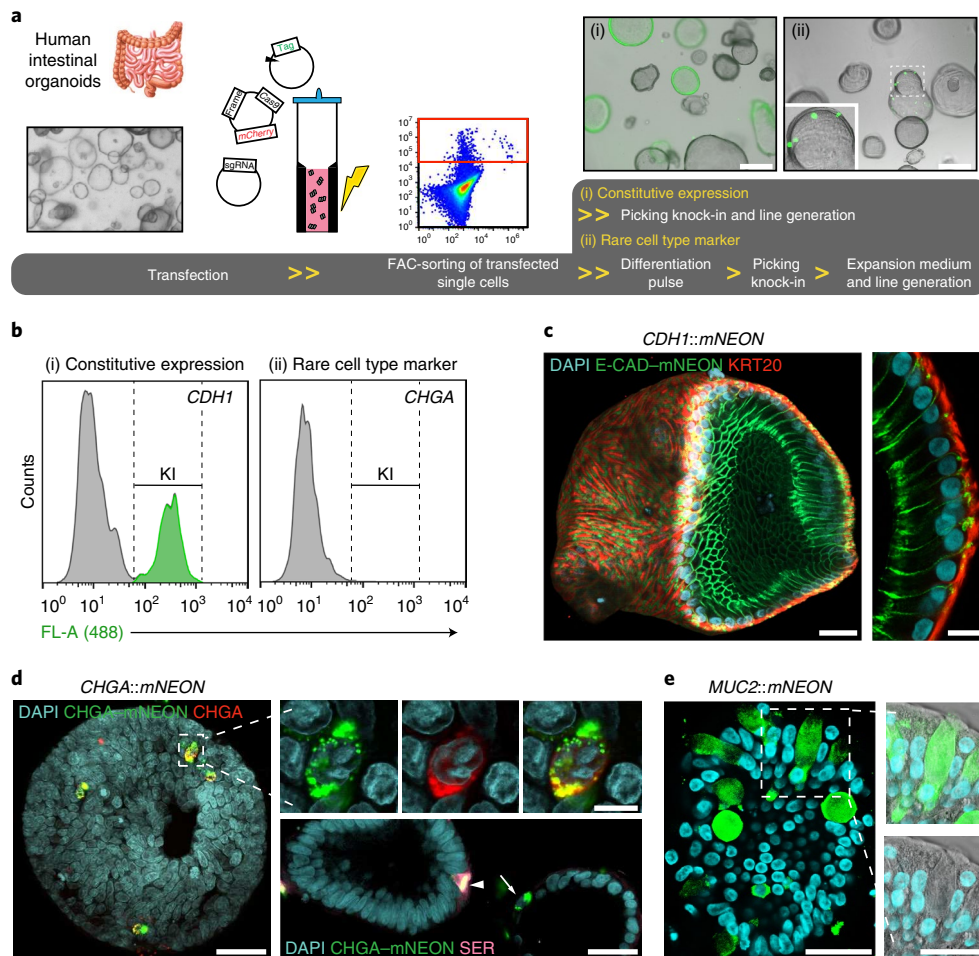


Fig. 4 | Labelling of different human intestinal cell types in organoids using CRISPR-HOT. **a**, Transfection and knock-in generation strategy for human intestinal organoids. Organoids are dissociated into small clumps of cells, mixed with DNA and electroporated in a cuvette. Single transfected cells are sorted using FACS and grown into organoids. When tagging constitutively expressed genes, single clonal tagged organoids are picked and used to establish clonal lines (i). To tag non-constitutively expressed differentiation markers, a reversible differentiation pulse with appropriate differentiation medium is used to visualize knocked-in organoids by the appearance of a few positive cells, which are subsequently picked and expanded in expansion medium to grow clonal lines (ii). **b**, Representative flow-cytometry histograms showing sorting of transfected cells in independent experiments in which *CDH1* and *CHGA* were targeted. Note that, whereas—in the case of *CDH1*—knocked-in cells were already visible during FACS analysis, for *CHGA*, no positive knocked-in cells were observed at this stage, as a differentiation pulse is required. **c**, Representative whole-mount image of a *CDH1::mNEON* organoid differentiated towards enterocytes and co-stained with KRT20 at low (left) and high magnification (right). **d**, Whole-mount staining of a *CHGA::mNEON* intestinal organoid for enteroendocrine cells stained for CHGA and serotonin (SER). The area indicated by the white dashed box is magnified on the right. The arrowhead indicates a *CHGA*⁺*SER*⁺ cell and the arrow indicates a *CHGA*⁺*SER*⁻ cell. **e**, Representative brightfield and fluorescence images of a *MUC2::mNEON* intestinal organoid reporter for goblet cells (right). Schematics of the *CDH1* and *CHGA* loci before and after knock-in and representative sequencing results of these lines is provided in Extended Data Figs. 3b,c and 8a. For **b–e**, all of the experiments were repeated at least twice independently with similar results. Scale bars, for **a**, 300 μ m; **c**, 50 μ m (left) and 20 μ m (right); **d**, 50 μ m (left), 10 μ m (top right) and 50 μ m (bottom right); and **e**, 50 μ m (left) and 25 μ m (right).

of the endogenously tagged *CDH1* enabled us to trace cell movement and dynamics. Analyses of time-lapse videos revealed that hepatocytes tend to organize around a central lumen and rotate around it while forming ‘rosette structures’ in the organoids (Extended Data Fig. 4).

We also established clonal *TUBB*-tagged hepatocyte organoids as a tool for tracing real-time mitotic spindle dynamics of proliferating hepatocytes (Fig. 5d, Extended Data Fig. 3e). Being able to generate lines with simultaneous tagging of more than one locus could be a major advantage for tracking such detailed and short-lived cellular changes. As concomitant visualization of the cell membrane and mitotic spindle would enable a more refined analysis of division events, we sequentially tagged *CDH1* with tdTomato in a *TUBB::mNEON* hepatocyte organoid line (Fig. 5a) and derived

double knocked-in *TUBB::mNEON*;*CDH1::tdTomato* clonal lines (Fig. 5e, Extended Data Fig. 3f).

Mitotic spindle analyses reveal an orchestrated mode of hepatocyte division. Hepatocytes in the liver are organized in a peculiar manner that reflects features of stratified, as well as monolayered (simple), epithelia³⁸. The positioning of mitotic spindle and the establishment of proper polarity and tissue organization are known to be linked, although exactly how this works in the liver is still a matter of debate^{39,40}. A recent study underscored that proper tissue architecture ensures correct mitotic spindle behaviour. Two-dimensional (2D) cultures of dissociated epithelial cells display defects in mitotic spindle behaviour as compared with what is observed when the same cells are cultured in a 3D configuration⁴¹. Human hepatocyte

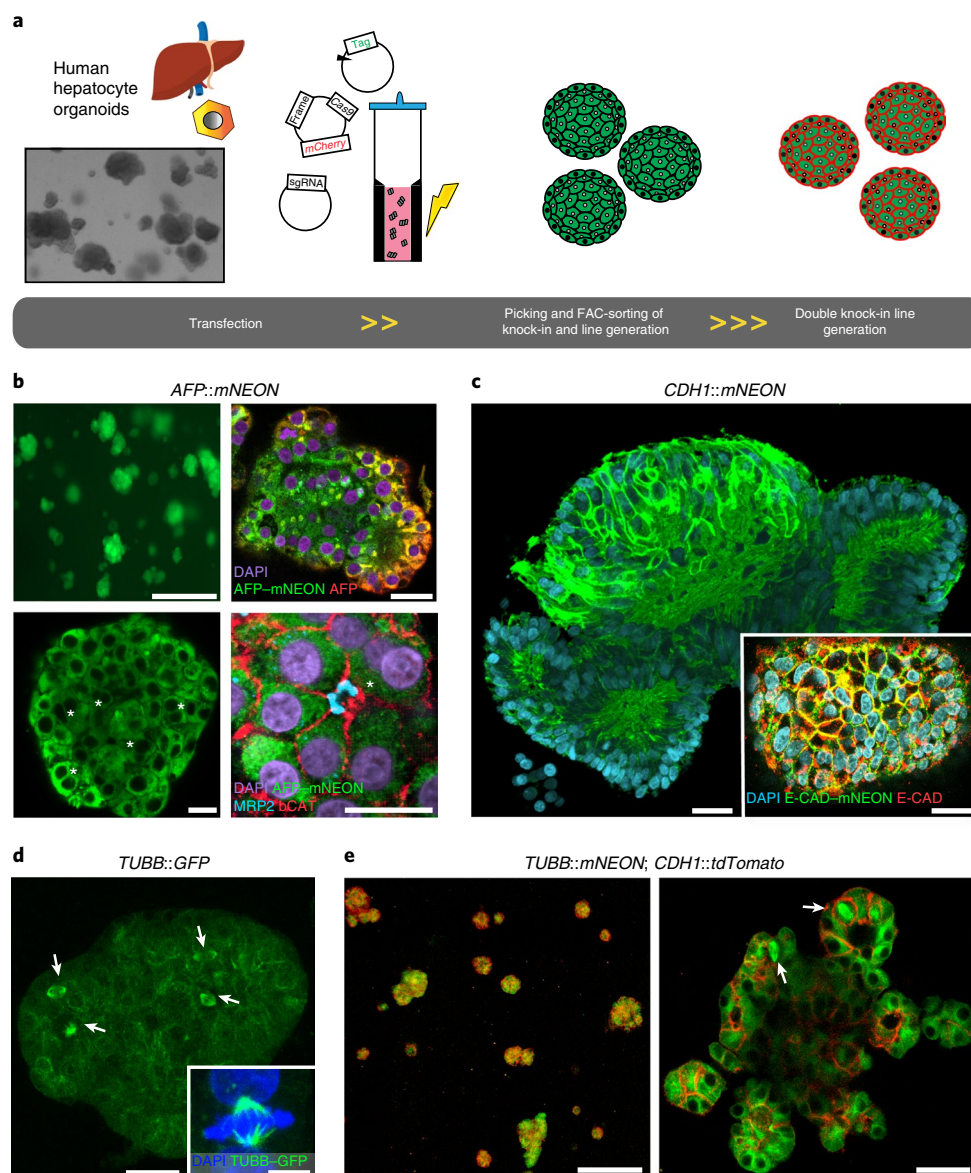


Fig. 5 | Generation of human hepatocyte reporter organoid lines using CRISPR-HOT. **a**, Transfection and knock-in strategy for human hepatocyte organoids. Organoids are dissociated into small clumps of cells, mixed with DNA and electroporated in a cuvette. Single transfected cells grow into organoids, which can be picked to establish clonal lines. An additional locus can eventually be targeted using the same procedures to establish double-knock-in reporters. **b**, Representative image of a clonal *AFP::mNEON* line. Co-staining of AFP-mNEON with an anti-AFP antibody demonstrates overlapping signal but limited penetration of the antibody. Note the typical hepatocyte polarity visualized by staining for the bile canalicular marker MRP2, while the cell membrane is marked by β -catenin. The asterisks indicate the presence of polyploid (binucleated) hepatocytes. The *AFP* locus was targeted in one independent experiment, resulting in multiple clonal *AFP-mNEON*⁺ organoids. **c**, Representative image of a *CDH1::mNEON* hepatocyte organoid. Inset: antibody staining for E-cadherin demonstrates perfect overlap with E-CAD-mNEON. The *CDH1* locus was targeted in four independent experiments. **d**, Representative image of a *TUBB::GFP* hepatocyte organoid. Inset: a dividing cell; the mitotic spindle was visualized by TUBB-GFP fluorescence and chromatin was visualized by staining for DAPI. The *TUBB* locus was targeted in five independent experiments. **e**, Representative image of a clonal *TUBB::mNEON; CDH1::tdTomato* double-knock-in hepatocyte line (left) and high-magnification imaging of a respective organoid (right). The double knock-in line was generated in one independent experiment. For **d** and **e**, the arrows indicate mitotic events. A schematic overview of the *AFP*, *TUBB* and *CDH1* loci before and after knock-in and representative sequencing results of these lines is provided in Extended Data Figs. 3d–f and 8a. Scale bars, for **b**, 500 μ m (top left), 50 μ m (top right) and 25 μ m (bottom left and right); **c**, 50 μ m and 25 μ m (inset); **d**, 25 μ m and 10 μ m (inset); and **e**, 500 μ m (left) and 50 μ m (right).

organoids retain cellular polarization, with an apical domain defined by the expression of MRP2 and ZO-1 (ref. ³²), facing the internal bile canaliculus (Fig. 5b). Our lines expressing endogenously tagged TUBB enabled us to analyse the behaviour of mitotic spindle in non-transformed human hepatocytes within a 3D structure. We performed time-lapse analyses (Supplementary Video 1)

and measured changes in spindle position as defined by the angle of rotation of spindle axis over time from metaphase to telophase (Fig. 6a, Extended Data Fig. 5a). We noticed that the spindle position is not static but, rather, can vary considerably. In particular, we observed that spindles that have a similar position in prometaphase and cytokinesis (arbitrarily defined as a difference of less than a 45°

angle between the two stages) hardly rotate (Fig. 6b, top). By contrast, spindles that change their axis between prometaphase and cytokinesis tended to rotate considerably over time (Fig. 6b, bottom), possibly trying to reach a specific orientation. Moreover, we measured the spindle position over time relative to the apical domain, which could be visualized by the presence of internal lumina. For this analysis, we defined the spindle axis and considered the angle that it forms with the apical side (Fig. 6c,d). The orientation of the spindle seemed to be random at prometaphase and during the subsequent mitotic stages, before cytokinesis, the orientation of the spindle consistently ended up within an angle between 0° and 45° relative to the apical side (Fig. 6e). Importantly, these conclusions were derived from multiple independent experiments using two donors that displayed similar behaviour. Taken together, these observations suggest that, at telophase, the position of the spindle is not random and that hepatocytes dividing next to a lumen undergo symmetric division with respect to the apicobasal axis, as confirmed by time-lapse analysis of cell division in the *CDH1::mNEON* line (Fig. 6f).

The liver is characterized by the presence of polyploid hepatocytes. These cells generally tend to increase in number with age and after injury⁴². Previous studies have suggested that polyploid hepatocytes predominantly originate from incomplete cytokinesis^{43,44}. Using our double *TUBB::mNEON*; *CDH1::tdTomato* hepatocyte organoid knock-in line, we observed (Supplementary Video 2) that the vast majority of mitotic events (>95%) originated from diploid hepatocyte division (Fig. 6g). In a small percentage of events (2–3%), we observed the formation of a binucleated cell from the division of a mononucleated cell. Interestingly, although the daughter cells appeared to be segregated—as marked by an initial formation of an E-CAD–tdTomato⁺ cell membrane separating the two—this transient border disappeared, resulting in a binucleated cell (Fig. 6g). We observed extremely rare (<1%) mitotic events encompassing the division of binucleated cells through a three-polar spindle. Division resulted in the formation of a mononucleated and binucleated cell (Fig. 6g). In these cases, the formation of the binucleated cell was also preceded by a transient E-CAD–tdTomato⁺ border between two of the daughter cells (Fig. 6g). In addition to rare multipolar spindles, we noted occasional formation of monopolar spindles, but such cells did not complete division and eventually died (Extended Data Fig. 5b–d).

Loss of TP53 induces aberrant mitotic spindle behaviour in human hepatocytes. TP53 is critical for maintaining genomic stability, and loss of TP53 is associated with increased polyploidy and aneuploidy^{45,46}. However, the specific role of TP53 in the behaviour of mitotic spindle is not fully understood. Here we combined CRISPR–HOT with CRISPR–Cas9-mediated gene knock-out to study the impact of loss of TP53 in our human hepatocyte lines expressing tagged TUBB (Fig. 7a). TP53-mutated organoids were picked on the basis of resistance to Nutlin-3a, clonally expanded and subsequently sequenced, revealing the presence of frameshift indels (Fig. 7a). When performing time-lapse analyses on these clonal lines, we frequently observed hepatocyte divisions associated with the formation of non-canonical mitotic spindles (Fig. 7b–f, Extended Data Fig. 6, Supplementary Video 3). In particular, we detected an increase in multipolar spindle formation that seemed to result from the division of hepatocytes with increased ploidy (Fig. 7c, Extended Data Fig. 6). In contrast to wild-type hepatocyte organoids, we observed the presence of polyploid hepatocytes with increased nuclei (3–4) per cell in these TP53-deficient organoids, which retained the ability to divide (Fig. 7c). Moreover, microtubules frequently appeared to be disorganized, for example, leading to a transient collapse of the mitotic spindle, yet these cells continued to divide (Fig. 7d, Extended Data Fig. 6). We observed these aberrations in multiple clonal TP53^{−/−} hepatocyte lines expressing tagged TUBB from two different donors. Notably, division of hepatocytes with these non-canonical mitotic spindles was not associated with loss of the internal lumina, neither did the loss of TP53

change proliferation rates (Extended Data Fig. 7a–c). Together, these results imply that TP53 is of critical importance for the integrity of mitotic spindle and its loss is associated with the formation and division of polyploid hepatocytes.

Discussion

Here we show that NHEJ can consistently mediate precise gene insertion with high efficiency in human organoids derived from different tissues. The strategy outperforms HDR, even when combined with transient TP53 inhibition. Importantly, as the knock-in efficiencies were assessed in wild-type primary human cells, they probably reflect the activities of these DNA repair pathways *in vivo*. These results are therefore more representative than the ones obtained in immortalized cell lines with highly divergent genomes. NHEJ-mediated knock-in appeared to be extremely precise, as observed in few studies previously²⁵. Furthermore, in the majority of cases the other allele appeared to be intact.

By exploiting this mechanism of cellular DNA repair, we were able to target different loci in organoids derived from multiple healthy human tissues (Extended Data Fig. 8). This was not restricted to tagging highly expressed genes—we could also tag non-constitutively expressed markers for rare cell types. To further facilitate this, we constructed different targeting plasmids that have a built-in selection strategy under the control of an independent promoter (Extended Data Fig. 1). This could help with the selection of knock-in events at non-constitutively expressed loci, of which expression cannot be induced by transient differentiation as performed in this study for *CHGA* and *MUC2*. In principle, such a built-in selection strategy could be important in the case of tagging genes with non-fluorescent tags.

Previously, there has been attention to analysing the mode of division of hepatocytes to understand how the peculiar hepatocyte polarity in the liver is created and maintained³⁸. Our double *TUBB::mNEON*; *CDH1::tdTomato* organoid reporter line enabled us to observe the division process in wild-type human hepatocytes in real time, which was previously possible only in immortalized cell lines^{39,40}. We observed rare cases of the formation and division of polyploid hepatocytes, which appeared to involve transient formation of a membrane between the daughter cells that precedes a subsequent fusion event. Previous analyses of the division of 2D-cultured primary mouse hepatocytes suggested that polyploid hepatocytes can divide and reduce their ploidy by formation of multipolar spindles, known as reductive mitosis^{47,48}. Our observations confirm binucleated hepatocyte division as a rare event but, rather, suggest maintenance of the polyploid state. These discrepancies could be due to differences in 2D versus 3D culturing of the cells that have been shown to induce missegregation⁴¹ or, alternatively, due to differences between mice and humans.

We also show that CRISPR–HOT can be multiplexed with gene knock-out. It has previously been shown that TP53 is involved in regulating hepatocyte ploidy in homeostasis and after liver damage in mice⁴⁹. We found that loss of TP53 facilitates the division of polyploid cells and promotes abnormal mitotic spindle behaviour, which could result in aneuploidy. Although aneuploidy is frequently associated with cancer, aneuploidy in the liver has been speculated to promote adaptation to liver injury⁵⁰. However, the causal relationship between TP53 mutation and mitotic spindle aberrations suggests that the consequent aneuploidy may be linked to hepatocarcinogenesis.

In conclusion, CRISPR–HOT is a versatile strategy that can be used to achieve fast and efficient gene knock-in in human wild-type organoids. This approach is applicable to other human cell models, such as organoids derived from induced pluripotent stem cells and embryonic stem cells. Although successful knock-in has already been achieved in these systems using conventional HDR approaches^{51–53}, the use of a homology-independent-based strategy may increase the efficiency of knock-in generation. CRISPR–HOT

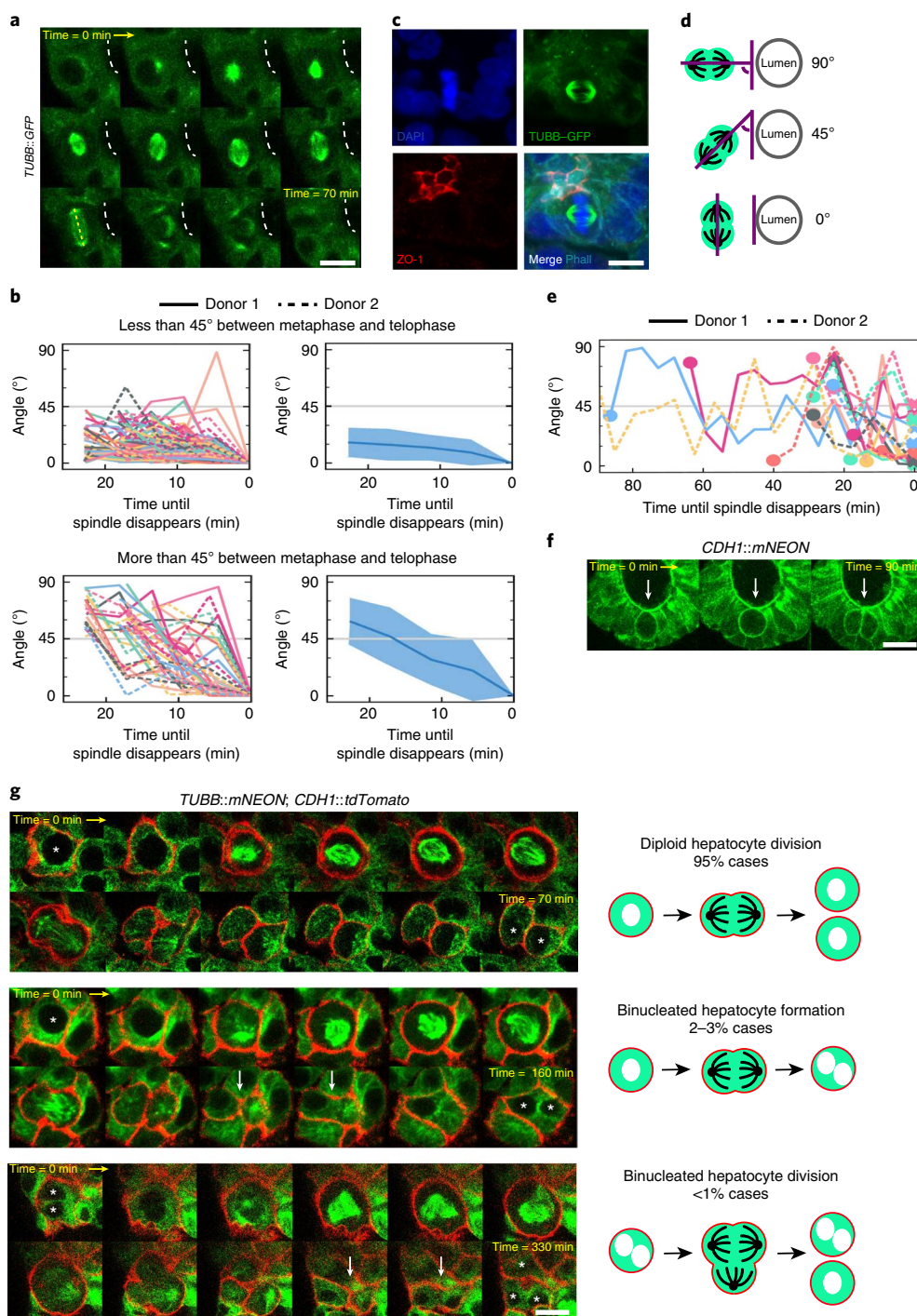


Fig. 6 | Mitotic spindle analyses in human hepatocyte reporter organoids reveal division dynamics. **a**, Time-lapse images (5 min interval) of a *TUBB::GFP* organoid visualized a hepatocyte dividing next to lumen (white dashed line). The spindle (yellow dashed line) ends up parallel to the apical luminal side. Mitotic events from 15 organoids from two different donors were analysed within eight independent experiments with similar results. **b**, Analysis of the spindle rotation in hepatocytes from metaphase to telophase. Mitotic spindles with a starting angle differing less than 45° (top) or more than 45° (bottom) from the final angle. The spindle angle is defined as the positioning of the spindle axis relative to the final positioning (defined as 0°). Each line represents one mitotic spindle; mitosis was analysed on the basis of two different donors. For the plots on the right, the centre line indicates the average spindle rotation relative to the final angle and the shading represents the s.d. from the average. **c**, Staining for the apical marker ZO-1 in *TUBB::GFP* organoids. **d**, Schematic of possible orientations of the mitotic spindle position at telophase relative to the lumen. **e**, Analysis of the spindle rotation of mitotic hepatocytes relative to the apical side. Each line represents one mitotic spindle; mitosis was analysed in cells from two different donors. The circles indicate metaphase and the crosses indicate telophase. **f**, Time-lapse imaging (interval, 45 min) of *CDH1::mNEON* organoids revealed that hepatocyte division occurs at the apical side and results in symmetric cell division. The experiment was repeated four times independently with similar results. **g**, Representative images of a time-lapse imaging experiment (interval, 5 min) in the double *TUBB::mNEON*; *CDH1::tdTomato* human hepatocyte organoid reporter line, showing examples of diploid hepatocyte division (top), binucleated hepatocyte formation (middle) and binucleated hepatocyte division (bottom). The asterisks indicate nuclei. The white arrows indicate the transiently formed E-CAD-tdTomato membrane. Mitotic events from 18 organoids were analysed within four independent experiments with similar results. Scale bars, for **a**, 10 μm ; **c**, 10 μm ; **f**, 20 μm ; and **g**, 10 μm . Source data are available online.

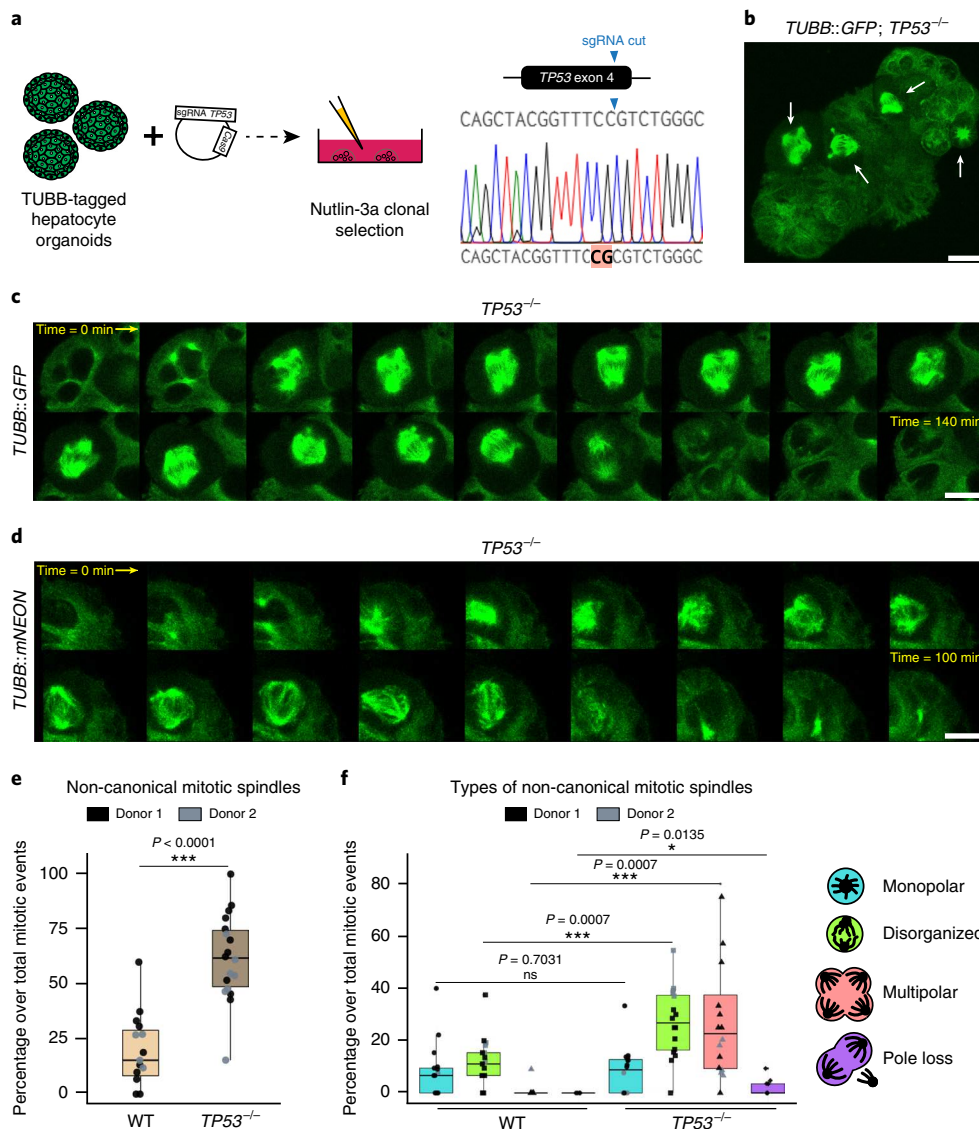


Fig. 7 | Loss of *TP53* causes mitotic spindle aberrations in human hepatocytes. **a**, Strategy for mutating *TP53* in TUBB-tagged hepatocyte organoids. A representative sequencing result from a clonal TUBB-tagged *TP53^{-/-}* hepatocyte organoid line (a homozygous frameshift indel as indicated by the red highlighted bases). Three clonal lines from each of two donors were sequenced and found to carry mutations in *TP53*. **b**, *TP53* mutations cause frequent non-canonical mitotic spindles. The arrows indicate a mitotic spindle. **c, d**, Representative images of a time-lapse imaging experiment (interval, 5 min) in TUBB-tagged *TP53^{-/-}* organoids demonstrate the division of a polyploid hepatocyte with three nuclei through the formation of a multipolar spindle (**c**) and the presence of a spindle with disorganized microtubules (**d**). For **b–d**, mitotic events in a total of 17 TUBB-tagged *TP53^{-/-}* hepatocyte organoids from two different donors were analysed within five independent experiments with similar results. **e**, Quantification of the percentage of non-canonical mitotic spindles in TUBB-tagged WT and *TP53^{-/-}* organoids. Each dot (n) represents the percentage of total mitotic aberrations normalized over the number of spindles quantified in one organoid. Donor 1, WT: $n = 11$; donor 2, WT: $n = 4$; donor 1, *TP53^{-/-}*: $n = 11$; donor 2, *TP53^{-/-}*: $n = 7$ biological independent experiments from TUBB-tagged WT and three clonal *TP53^{-/-}* lines from each of the two different donors analysed. **f**, Analysis of the type of non-canonical mitotic spindles. Each dot (n) represents the percentage of a type of mitotic aberration normalized to the total number of spindles quantified in one organoid. Donor 1, WT: $n = 12$; donor 2, WT: $n = 4$; donor 1, *TP53^{-/-}*: $n = 11$; donor 2, *TP53^{-/-}*: $n = 5$ biological independent experiments from TUBB-tagged WT and three clonal *TP53^{-/-}* lines from each of the two different donors analysed. For **e** and **f**, statistical analysis was performed using two-sided unpaired t -tests; * $P < 0.05$; ** $P < 0.01$; *** $P < 0.001$. For the box plots in **e** and **f**, the boxes indicate the 25–75th percentiles, the centre line indicates the mean and the lines indicate the minimum and maximum values. Scale bars, for **b**, 25 μm ; **c**, 10 μm ; and **d**, 10 μm . Source data are available online.

constitutes a useful asset in studies that require the generation of reporter lines, protein tagging, labelling of cellular structures and lineage tracing experiments.

Online content

Any methods, additional references, Nature Research reporting summaries, source data, extended data, supplementary information,

acknowledgements, peer review information; details of author contributions and competing interests; and statements of data and code availability are available at <https://doi.org/10.1038/s41556-020-0472-5>.

Received: 13 June 2019; Accepted: 20 January 2020;
Published online: 2 March 2020

References

- Clevers, H. Modeling development and disease with organoids. *Cell* **165**, 1586–1597 (2016).
- Rossi, G., Manfrin, A. & Lutolf, M. P. Progress and potential in organoid research. *Nat. Rev. Genet.* **19**, 671–687 (2018).
- Artegiani, B. & Clevers, H. Use and application of 3D-organoid technology. *Hum. Mol. Genet.* **27**, R99–R107 (2018).
- Farin, H. F. et al. Visualization of a short-range Wnt gradient in the intestinal stem-cell niche. *Nature* **530**, 340–343 (2016).
- Tetteh, P. W. et al. Replacement of lost Lgr5-positive stem cells through plasticity of their enterocyte-lineage daughters. *Cell Stem Cell* **18**, 203–213 (2016).
- Barriga, F. M. et al. Mex3a marks a slowly dividing subpopulation of Lgr5⁺ intestinal stem cells. *Cell Stem Cell* **20**, 801–816 (2017).
- Kon, S. et al. Cell competition with normal epithelial cells promotes apical extrusion of transformed cells through metabolic changes. *Nat. Cell Biol.* **19**, 530–541 (2017).
- Beumer, J. et al. Enteroendocrine cells switch hormone expression along the crypt-to-villus BMP signalling gradient. *Nat. Cell Biol.* **20**, 909–916 (2018).
- Serra, D. et al. Self-organization and symmetry breaking in intestinal organoid development. *Nature* **569**, 66–72 (2019).
- Gehart, H. et al. Identification of enteroendocrine regulators by real-time single-cell differentiation mapping. *Cell* **176**, 1158–1173 (2019).
- Drost, J. et al. Sequential cancer mutations in cultured human intestinal stem cells. *Nature* **521**, 43–47 (2015).
- Drost, J. et al. Use of CRISPR-modified human stem cell organoids to study the origin of mutational signatures in cancer. *Science* **358**, 234–238 (2017).
- Artegiani, B. et al. Probing the tumor suppressor function of BAP1 in CRISPR-engineered human liver organoids. *Cell Stem Cell* **24**, 927–943 (2019).
- Matano, M. et al. Modeling colorectal cancer using CRISPR-Cas9-mediated engineering of human intestinal organoids. *Nat. Med.* **21**, 256–262 (2015).
- Schwank, G. et al. Functional repair of CFTR by CRISPR/Cas9 in intestinal stem cell organoids of cystic fibrosis patients. *Cell Stem Cell* **13**, 653–658 (2013).
- Shimokawa, M. et al. Visualization and targeting of LGR5⁺ human colon cancer stem cells. *Nature* **545**, 187–192 (2017).
- Cortina, C. et al. A genome editing approach to study cancer stem cells in human tumors. *EMBO Mol. Med.* **9**, 869–879 (2017).
- Sugimoto, S. et al. Reconstruction of the human colon epithelium in vivo. *Cell Stem Cell* **22**, 171–176 (2018).
- Essers, J. et al. Analysis of mouse *Rad54* expression and its implications for homologous recombination. *DNA Repair* **1**, 779–793 (2002).
- Hustedt, N. & Durocher, D. The control of DNA repair by the cell cycle. *Nat. Cell Biol.* **19**, 1–9 (2016).
- Haapaniemi, E., Botla, S., Persson, J., Schmierer, B. & Taipale, J. CRISPR-Cas9 genome editing induces a p53-mediated DNA damage response. *Nat. Med.* **24**, 927–930 (2018).
- Ihry, R. J. et al. p53 inhibits CRISPR-Cas9 engineering in human pluripotent stem cells. *Nat. Med.* **24**, 939–946 (2018).
- Schirotti, G. et al. Precise gene editing preserves hematopoietic stem cell function following transient p53-mediated DNA damage response. *Cell Stem Cell* **24**, 551–565 (2019).
- Betermier, M., Bertrand, P. & Lopez, B. S. Is non-homologous end-joining really an inherently error-prone process? *PLoS Genet.* **10**, e1004086 (2014).
- Guo, T. et al. Harnessing accurate non-homologous end joining for efficient precise deletion in CRISPR/Cas9-mediated genome editing. *Genome Biol.* **19**, 170 (2018).
- Auer, T. O., Duroure, K., De Cian, A., Concordet, J. P. & Del Bene, F. Highly efficient CRISPR/Cas9-mediated knock-in in zebrafish by homology-independent DNA repair. *Genome Res.* **24**, 142–153 (2014).
- Suzuki, K. et al. In vivo genome editing via CRISPR/Cas9 mediated homology-independent targeted integration. *Nature* **540**, 144–149 (2016).
- Lackner, D. H. et al. A generic strategy for CRISPR-Cas9-mediated gene tagging. *Nat. Commun.* **6**, 10237 (2015).
- Schmid-Burgk, J. L., Honing, K., Ebert, T. S. & Hornung, V. CRISPaint allows modular base-specific gene tagging using a ligase-4-dependent mechanism. *Nat. Commun.* **7**, 12338 (2016).
- He, X. et al. Knock-in of large reporter genes in human cells via CRISPR/Cas9-induced homology-dependent and independent DNA repair. *Nucleic Acids Res.* **44**, e85 (2016).
- Huch, M. et al. Long-term culture of genome-stable bipotent stem cells from adult human liver. *Cell* **160**, 299–312 (2015).
- Hu, H. et al. Long-term expansion of functional mouse and human hepatocytes as 3D organoids. *Cell* **175**, 1591–1606 (2018).
- Okita, K. et al. An efficient nonviral method to generate integration-free human-induced pluripotent stem cells from cord blood and peripheral blood cells. *Stem Cells* **31**, 458–466 (2013).
- Sato, T. et al. Long-term expansion of epithelial organoids from human colon, adenoma, adenocarcinoma, and Barrett's epithelium. *Gastroenterology* **141**, 1762–1772 (2011).
- Fujii, M. et al. Human intestinal organoids maintain self-renewal capacity and cellular diversity in niche-inspired culture condition. *Cell Stem Cell* **23**, 787–793 (2018).
- Fujii, M., Matano, M., Nanki, K. & Sato, T. Efficient genetic engineering of human intestinal organoids using electroporation. *Nat. Protoc.* **10**, 1474–1485 (2015).
- Yin, X. et al. Niche-independent high-purity cultures of Lgr5⁺ intestinal stem cells and their progeny. *Nat. Methods* **11**, 106–112 (2014).
- Treyer, A. & Musch, A. Hepatocyte polarity. *Compr. Physiol.* **3**, 243–287 (2013).
- Wang, T., Yanger, K., Stanger, B. Z., Cassio, D. & Bi, E. Cytokinesis defines a spatial landmark for hepatocyte polarization and apical lumen formation. *J. Cell Sci.* **127**, 2483–2492 (2014).
- Lazaro-Dieguez, F. & Musch, A. Cell-cell adhesion accounts for the different orientation of columnar and hepatocytic cell divisions. *J. Cell Biol.* **216**, 3847–3859 (2017).
- Knouse, K. A., Lopez, K. E., Bachofner, M. & Amon, A. Chromosome segregation fidelity in epithelia requires tissue architecture. *Cell* **175**, 200–211 (2018).
- Wang, M. J., Chen, F., Lau, J. T. Y. & Hu, Y. P. Hepatocyte polyploidization and its association with pathophysiological processes. *Cell Death Dis.* **8**, e2805 (2017).
- Guidotti, J. E. et al. Liver cell polyploidization: a pivotal role for binuclear hepatocytes. *J. Biol. Chem.* **278**, 19095–19101 (2003).
- Margall-Ducos, G., Celton-Morizur, S., Couton, D., Bregerie, O. & Desdouets, C. Liver tetraploidization is controlled by a new process of incomplete cytokinesis. *J. Cell Sci.* **120**, 3633–3639 (2007).
- Aylon, Y. & Oren, M. p53: guardian of ploidy. *Mol. Oncol.* **5**, 315–323 (2011).
- Vogel, C., Kienitz, A., Hofmann, I., Muller, R. & Bastians, H. Crosstalk of the mitotic spindle assembly checkpoint with p53 to prevent polyploidy. *Oncogene* **23**, 6845–6853 (2004).
- Duncan, A. W. et al. The ploidy conveyor of mature hepatocytes as a source of genetic variation. *Nature* **467**, 707–710 (2010).
- Duncan, A. W. et al. Frequent aneuploidy among normal human hepatocytes. *Gastroenterology* **142**, 25–28 (2012).
- Kurinna, S. et al. p53 regulates a mitotic transcription program and determines ploidy in normal mouse liver. *Hepatology* **57**, 2004–2013 (2013).
- Duncan, A. W. et al. Aneuploidy as a mechanism for stress-induced liver adaptation. *J. Clin. Invest.* **122**, 3307–3315 (2012).
- Zhang, J. P. et al. Efficient precise knockin with a double cut HDR donor after CRISPR/Cas9-mediated double-stranded DNA cleavage. *Genome Biol.* **18**, 35 (2017).
- Mitzelfelt, K. A. et al. Efficient precision genome editing in iPSCs via genetic co-targeting with selection. *Stem Cell Rep.* **8**, 491–499 (2017).
- Zhang, J. Z. et al. A human iPSC double-reporter system enables purification of cardiac lineage subpopulations with distinct function and drug response profiles. *Cell Stem Cell* **24**, 802–811 (2019).

Publisher's note Springer Nature remains neutral with regard to jurisdictional claims in published maps and institutional affiliations.

© The Author(s), under exclusive licence to Springer Nature Limited 2020

Methods

Human organoid culturing. Human fetal livers (donor 1: female, 20 weeks gestational age; donor 2: gender unknown, 8 weeks gestational age) were obtained from Leiden University Medical Centre (MC). The use of these samples for research was approved by the Dutch Ethical Medical Council (Leiden University MC). Isolation, generation and culture of human hepatocytes were performed as described previously³². Human liver biopsies were obtained from anonymous healthy liver donors (age and gender not disclosed) at Erasmus MC Rotterdam with informed consent in accordance with the Declaration of Helsinki and Dutch law. Isolation, generation and human liver ductal organoids were performed as described previously³¹. Human ileal tissue (male, 37 years) was obtained from UMC Utrecht with informed consent in accordance with the Declaration of Helsinki and Dutch law. Biopsies were taken from the normal mucosa of a resected intestinal segment from an ileal neuroendocrine tumour. Human small intestinal crypts were isolated, processed and cultured as described previously³⁴. Intestinal organoids were cultured in standard culture conditions (ENR medium)³². Differentiation was achieved by supplementing ENR medium with γ -secretase inhibitor DAPT (10 μ M, Sigma Aldrich; for goblet cell enrichment), or by adding DAPT (10 μ M, Sigma Aldrich) and the MEK inhibitor PD0325901 (500 nM; Sigma Aldrich) and withdrawing the p38 MAPK inhibitor SB202190, the TGF- β inhibitor A83-01, nicotinamide and Wnt-conditioned medium from the ENR medium (for enteroendocrine cell enrichment), as described previously⁸. The collection of available tissue from patients or healthy donors with informed consent was approved by the Dutch Ethical Medical Councils (UMC Utrecht, Erasmus MC Rotterdam and Leiden University MC).

DNA plasmids. For the electroporation of human intestinal, hepatocyte and liver ductal organoids, different plasmids were used. The sgRNAs for the different targeted genes were cloned into the vector pSPgRNA (Addgene plasmid 47108) using a protocol that was described previously³⁴. Oligo sequences for each sgRNA were as follows: *AFP* fwd, 5'-CACCGTGCAGATTCTCAGCGCTGT-3'; *AFP* rev, 5'-AAACACAGGCTGAGAAATCTGCAC-3'; *CDH1* fwd, 5'-CACCGAGGCGGCGAGGACGACTAG-3'; *CDH1* rev, 5'-AAACCTAGTCGTCTCGCCGCTC-3'; *CHGA* fwd, 5'-CACCGCAGCTGCAGGCACTACGGCG-3'; *CHGA* rev, 5'-AAACCGCGTAGTGCCTGCAGTGC-3'; *KRT18* fwd, 5'-CACCGCAATGACACCAAAGTTCTG-3'; *KRT18* rev, 5'-AAACCAGAACTTTGGTGTCATTGGC-3'; *KRT19* fwd, 5'-CACCGCCCAAGGCTGCTGCCTCAG-3'; *KRT19* rev, 5'-AAACCTGAGGACGAGGCTCTGGG-3'; *MUC2* fwd, 5'-CACCGCATCTGGGAGCGGGTGAGC-3'; *MUC2* rev, 5'-AAACGCTCACCGCTCCCCAGATGC-3'; *TUBB* fwd, 5'-CACCGAGCGGCGAGGACGACTA-3'; *TUBB* rev, 5'-AAACTAGGCTCTCTCGGCCTC-3'.

The frame-selector plasmids containing a sgRNA that linearizes the donor-targeting construct, the *Cas9* and *mCherry* for detection of electroporated cells were obtained from Addgene (plasmids 66939, 66940 and 66941). The GFP and mNEON targeting vectors were obtained from V. Hornung²⁹. All other targeting constructs (for both HDR and NHEJ) used in this study are shown in Extended Data Fig. 1 and were either designed and cloned in this study. For the HDR targeting constructs, the tags were flanked by homology arms (length, 0.5 kb) for the specific genomic regions. To study the effect of transient TP53 inhibition on knock-in efficiency, a plasmid encoding a dominant negative form of TP53 (DN TP53; Addgene, 41856) was cotransfected with the respective plasmids.

Organoid transfection and generation of knock-in lines. Transfection of human liver ductal organoids was performed using an electroporation-based protocol that was described previously³³. In brief, the organoids were co-electroporated with the appropriate sgRNA plasmid, the frame selector plasmid and the targeting plasmid. Then, 2 d after electroporation, the transfected organoids were picked on the basis of mCherry expression (from the frame selector plasmid) and dissociated into single cells with accutase (Life technologies, 00-4555-56) and replated in a BME^R (AMSBIO, 3533-005-02) drop. Growing knocked-in organoids (determined on the basis of fluorescence expression) were picked and used to establish clonal knocked-in organoid lines. Wnt-surrogate³⁵ (0.15 nM, U-Protein Expression) and Rho Kinase inhibitor Y27632 (10 μ M, Calbiochem) were added to the medium whenever cells were at the single-cell stage to help recovery. For genotyping, organoids were lysed using a lysis buffer (0.1 M Tris-HCl pH 8.5, 0.2 M NaCl, 0.2% SDS, 0.05 M EDTA, 0.4 mg ml⁻¹ Proteinase K) and DNA was isolated by ethanol precipitation. PCR amplification followed by sequencing was used to confirm proper knock-in at the targeted locus. To analyse knock-in efficiency, cells from the different samples were isolated from the BME^R, digested into single cells with accutase and used for FACS analysis (FACS Aria, BD). DAPI was used to identify live cells. FlowJo software was used for data analyses.

Transfection of human hepatocyte organoids was performed by cuvette electroporation. Organoids were collected from 2 wells out of a 12-well plate and were dissociated into single cells/small clumps using accutase. After two washes with PBS, organoids were resuspended in 150 μ l of Opti-MEM and supplemented with the plasmids (10 μ g total dissolved in 20 μ l of PBS) and transferred into a 2 mm cuvette. Electroporation was performed using the following parameters on the NEPA21 electroporator: Poring Pulse (Voltage = 175 V, Pulse Length = 7.5 msec, Pulse Interval = 50 msec, Number of Pulse = 2), Transfer Pulse (Voltage = 20 V,

Pulse Length = 50 msec, Pulse Interval = 50 msec, Number of Pulse = 5). Complete medium supplemented with Rho Kinase inhibitor Y27632 (10 μ M, Calbiochem) was added to the cuvette. The cells were allowed to recover for 30 min, after which they were seeded in BME^R. Growing knocked-in organoids (determined on the basis of fluorescence expression) were picked and used to establish clonal human hepatocyte knock-in lines. To generate the TP53-mutant hepatocyte organoid lines, organoids expressing endogenously tagged TUBB were electroporated with a TP53sgRNA-Cas9-GFP plasmid¹¹ and clonal organoids with inactive TP53 were selected based on Nutlin-3a resistance by adding 10 μ M Nutlin-3a (Cayman Chemicals, 548472-68-0) to the medium. Clonal lines were established and each line was genotyped to confirm the presence of biallelic TP53 mutations. Three clonal TP53^{-/-} lines from two hepatocyte lines expressing tagged TUBB originating from two different donors were generated. For knock-in efficiency analysis, hepatocyte organoids were similarly electroporated and, 3 d after electroporation, cells were recovered from the BME^R and used for FACS analysis (FACS Aria, BD). DAPI was used to identify live cells. FlowJo was used for data analyses. Alternatively, to determine the preciseness of gene knock-in at the two different loci (*CDH1* and *TUBB*), single transfected cells were sorted using FACS and seeded in BME^R to grow out as single clonal organoids. Fluorescence images of entire 24-well plates were acquired and the number of fluorescence-positive and -negative organoids were quantified. Representative positive and negative organoids were picked and screened for their genotype using PCR amplification and subsequent sequencing.

Transfection of human intestinal organoids was performed by cuvette electroporation of a single well of a 12-well plate as described previously³⁶ using a NEPA21 electroporator (Nepa Gene). Then, 3–5 d after electroporation, single transfected cells were sorted using FACS (FACS Aria, BD) on the basis of transient expression of mCherry from the frame selector plasmid and seeded in BME^R. To generate knock-in lines of constitutively expressed genes, single growing organoids were picked on the basis of fluorescence to establish clonal lines. For the non-constitutively expressed genes, that is, *MUC2* and *CHGA*, a differentiation pulse of 24 h with the respective differentiation medium (compositions described above) was used. Single organoids showing a few fluorescence-positive induced cells were picked and transferred to expansion (ENR) medium for subsequent clonal line generation. In these clonal lines, differentiation to enrich for the specific differentiated intestinal cell types was performed by a switch from ENR to the respective differentiation medium for 5 d.

All of the knock-in organoid lines from the different organs were confirmed for their genotype by PCR amplification and subsequent sequencing. The generation of knock-in lines at different loci was repeated multiple times (more than three experiments) from at least two independent donors for human liver ductal and hepatocyte organoids, and one donor for human small intestinal organoids. A protocol to generate knock-in organoids is available at [Protocol Exchange](#)³⁶.

Whole-mount immunofluorescence. For whole-mount immunofluorescence staining, organoids were isolated from the BME^R using Cell Recovery Solution (Corning), fixed for 30 min to 1 h in 4% PFA, permeabilized, and blocked by incubation in 0.2% Triton X-100 and 5% normal donkey serum (Jackson Laboratories) in PBS for 1 h at room temperature. Alternatively, staining was performed directly in the culture plate without dissociation of the BME^R drop and following the same procedure. Primary antibodies were incubated at 4 °C overnight. The antibodies used in this study were as follows: anti-AFP rabbit polyclonal 1:250 (Thermo Fisher Scientific PA5-16658), anti-chromogranin A rabbit polyclonal 1:200 (Labnet, LN1401487), anti-cleaved caspase-3 (Asp 175) rabbit polyclonal 1:400 (Cell Signaling Technology, 9661L), anti-E-cadherin mouse monoclonal 1:200 (BD Bioscience, 610182), anti-keratin19 mouse monoclonal 1:200 (Cell Signalling, 4558S), anti-keratin20 mouse monoclonal 1:200 (Neomarkers, MS-377-S1), anti-MRP2 mouse monoclonal 1:100 (Abcam, ab3373), anti-serotonin goat polyclonal 1:200 (Abcam, ab66047), anti-ZO-1 rabbit polyclonal 1:200 (Life technology, 402200). After washing with PBS, Alexa Fluor-conjugated secondary antibodies 1:1,000 (Thermo Fisher Scientific, A10037, A10042 and A31573) were added for 1 h at room temperature. Phalloidin-Atto 647N 1:1,000 (Sigma Aldrich, 65906) was used for actin staining. DAPI was used to counterstain nuclei. Organoids were mounted and imaged using an Sp8 confocal microscope (Leica). The images were processed using Photoshop CS4 or ImageJ. Imaris was used for the 3D-reconstruction and visualization of images.

Time-lapse imaging. For time-lapse microscopy imaging, organoids were passaged 2 d before imaging and seeded onto glass-bottom plates (Greiner, 662892). All imaging was performed using an Sp8 confocal microscope (Leica), which was continuously held at 37 °C and equipped with a culture chamber for overflow of 5% CO₂, except for one single experiment, where organoids were imaged using a spinning disk microscope (Nikon). Imaging of the CDH1⁻, TUBB⁻, and double CDH1/TUBB-tagged hepatocyte organoids was performed for up to 72 h, with acquisition intervals of 5 min or 15 min and z-stack steps of 4 μ m. For fluorescence detection, we used minimal amounts of excitation light. ImageJ was used to assemble the videos and for image analysis. At least two different clonal lines were imaged and four independent imaging experiments were performed. Quantification of mitosis and types of non-canonical mitotic spindles was performed on the imaging of 15 organoids from the 3 different clonal lines

derived from 2 different donors in independent experiments and was blindly assessed by 2 researchers.

Imaging analysis. To analyse mitotic spindle, every spindle that was visible at any *xy*-plane was analysed. The coordinates of both ends of the spindle (spindle poles) were manually tracked over time. The spindle was tracked from the moment that both ends were clearly separated (metaphase) to the moment just before the spindle disappeared (telophase). The 2D orientation of the line segment between both ends was calculated for each time point, ignoring the *z* coordinate of the ends. For all spindles that were clearly rotating next to an internal lumen, the position on the edge of the lumen closest to the spindle was manually recorded. The rotation of mitotic spindles in the TUBB-tagged organoids was analysed using custom-written Python scripts (available from the corresponding author on request). Analysis of modes of cell division in the double CDH1/TUBB-tagged line was performed by tracing single mitotic events using ImageJ.

Cell movement in the CHD1-tagged organoids was traced manually. The position of the cell centroid was determined on the basis of cell membrane labelling and was registered at every time point. The cells were selected such that every part of the organoid had its motion sampled. Arrows were then drawn from the position of a cell centroid at the first time point, pointing to its position at the last time point. For presentation purposes, the arrows indicate their 2D orientation, ignoring the *z* position of the cells. Absolute average cell rotation degrees were calculated by averaging the movement of single cells within one organoid.

Statistics and reproducibility. All data analyses, quantifications and statistical evaluations were performed using Rstudio. Data visualization was performed in Rstudio using the ggplot2 package. Experiments were performed at least three times, unless stated otherwise. The reproducibility, sample sizes and, where appropriate, statistical analyses are described in the figure legends. Source data are available online.

Reporting Summary. Further information on research design is available in the Nature Research Reporting Summary linked to this article.

Data availability

Plasmids generated in this study (Extended Data Fig. 1) are deposited in Addgene (138567, 138568, 138569, 138570 and 138571). Genotyping data that support the findings of this study have been deposited in GenBank under the following accession codes: MN952225, MN952226, MN952227, MN952228, MN952229, MN952230, MN952231 and MN952232. All other data supporting the findings of this study are available from the corresponding author on reasonable request. Source data for Figs. 1, 2, 6 and 7, and Extended Data Figs. 2, 4 and 7 are presented with this paper.

Code availability

Custom-written Python scripts that were used to analyse the rotation of mitotic spindles are available from the corresponding author on request.

References

54. Ran, F. A. et al. Genome engineering using the CRISPR–Cas9 system. *Nat. Protoc.* **8**, 2281–2308 (2013).
55. Janda, C. Y. et al. Surrogate Wnt agonists that phenocopy canonical Wnt and β -catenin signalling. *Nature* **545**, 234–237 (2017).
56. Artegiani, B. et al. Generation of knock-in human organoids by CRISPR–HOT. *Protoc. Exch.* <https://doi.org/10.21203/rs.2.20352/v1> (2020).

Acknowledgements

We thank G. Darmasaputra for help with imaging and analyses of polyploid divisions and M. Galli for advice on hepatocyte ploidy; Y. Bar-Ephraïm and J. Bernink for help with FACS; H. Gehart and V. Hornung for providing plasmids; and S. van den Brink for support with preparation of medium components. We acknowledge all of the anonymous tissue donors. This work is part of the OncoCode Institute, which is partly financed by the Dutch Cancer Society. B.A. was supported by a FEBS long-term fellowship and is the recipient of a VENI grant (NWO-ALW 863.15.015).

Author contributions

Conceptualization: B.A. and D.H.; methodology: B.A., D.H. and H.C.; software: B.A., D.H., R.K. and X.Z.; formal analysis: B.A., D.H., R.K. and X.Z.; investigation: B.A., D.H., J.B., R.K., I.J. and X.Z.; resources: S.C.v.S.L., S.T., J.v.Z. and H.C.; data curation: B.A., D.H. and R.K.; writing—original draft: B.A., D.H. and H.C.; writing—review and editing: B.A., D.H., J.B., R.K., X.Z. and H.C.; visualization: B.A., D.H. and R.K.; supervision: H.C.; project administration: B.A. and D.H.; and funding acquisition: B.A., S.T., J.v.Z. and H.C. B.A. and D.H. contributed equally as joint first authors. J.B. and R.K. contributed equally as joint second authors.

Competing interests

H.C. holds several patents on organoid technology. Their application numbers, followed by their publication numbers (if applicable), are as follows: PCT/NL2008/050543, WO2009/022907; PCT/NL2010/000017, WO2010/090513; PCT/IB2011/002167, WO2012/014076; PCT/IB2012/052950, WO2012/168930; PCT/EP2015/060815, WO2015/173425; PCT/EP2015/077990, WO2016/083613; PCT/EP2015/077988, WO2016/083612; PCT/EP2017/054797, WO2017/149025; PCT/EP2017/065101, WO2017/220586; PCT/EP2018/086716, n/a; and GB1819224.5, n/a.



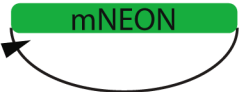


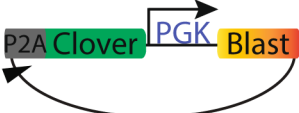



Additional information

Extended data is available for this paper at <https://doi.org/10.1038/s41556-020-0472-5>.

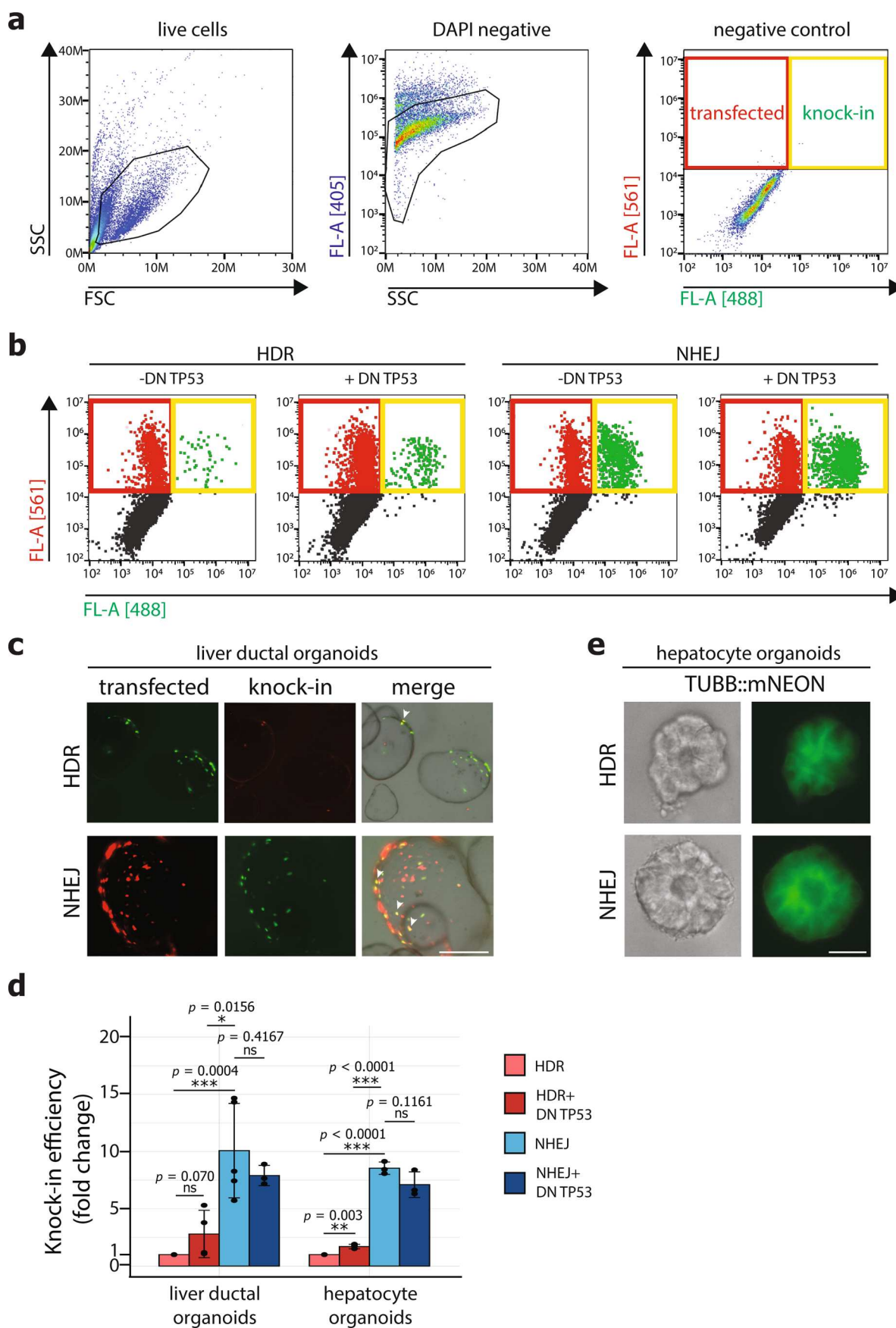
Supplementary information is available for this paper at <https://doi.org/10.1038/s41556-020-0472-5>.

Correspondence and requests for materials should be addressed to H.C.

Reprints and permissions information is available at www.nature.com/reprints.

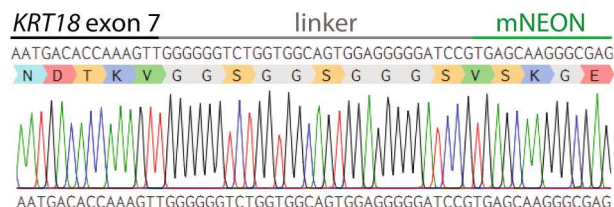
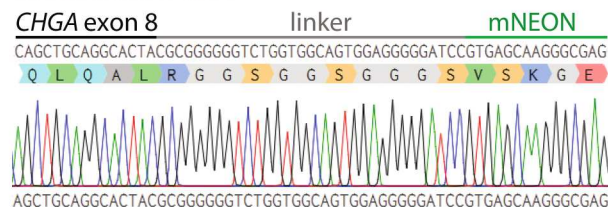
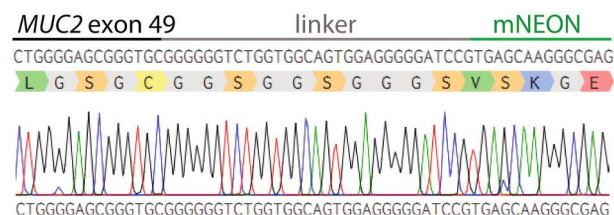
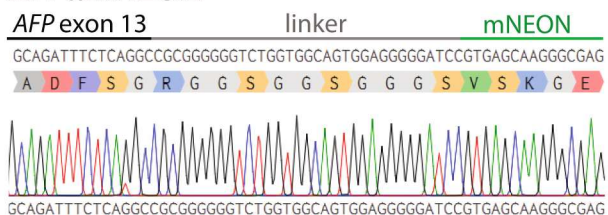
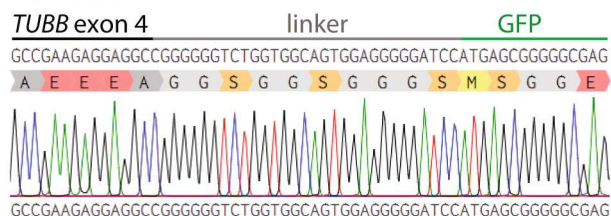
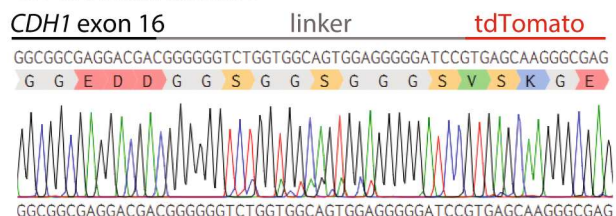
<p>Targeting vectors HDR</p> <p>KRT19 tdTomato targeting plasmid</p>  <p>TUBB mNEON targeting plasmid</p> 	<p>Application</p> <p>for KRT19 C-term tagging with tdTomato</p> <p>for TUBB C-term tagging with mNEON</p>	<p>Source</p> <p>this study</p> <p>this study</p>
<p>Universal targeting vectors NHEJ</p> <p>self-cleaving mNEON plasmid</p>  <p>self-cleaving GFP plasmid</p>  <p>self-cleaving tdTomato plasmid</p>  <p>self-cleaving P2A Clover BlastR plasmid</p>  <p>self-cleaving Clover BlastR plasmid</p>  <p>self-cleaving double frame mNEON plasmid</p>  <p>self-cleaving double frame plasmid</p> 	<p>Application</p> <p>for protein C-term tagging with mNEON</p> <p>for protein C-term tagging with GFP</p> <p>for protein C-term tagging with tdTomato</p> <p>for protein expression detection by Clover and build-in selection strategy</p> <p>for protein C-term tagging with Clover and build-in selection strategy</p> <p>for protein C-term or N-term tagging with mNEON</p> <p>for insertion of a tag of interest in the double frame plasmid</p>	<p>Source</p> <p>Ref. 27</p> <p>Ref. 27</p> <p>this study</p> <p>this study</p> <p>this study</p> <p>this study</p>

Extended Data Fig. 1 | Schematic overview of NHEJ and HDR targeting plasmids used in this study. List of plasmids used or generated in this study for gene tagging, including a schematic map of the plasmid, the application and the plasmid source.

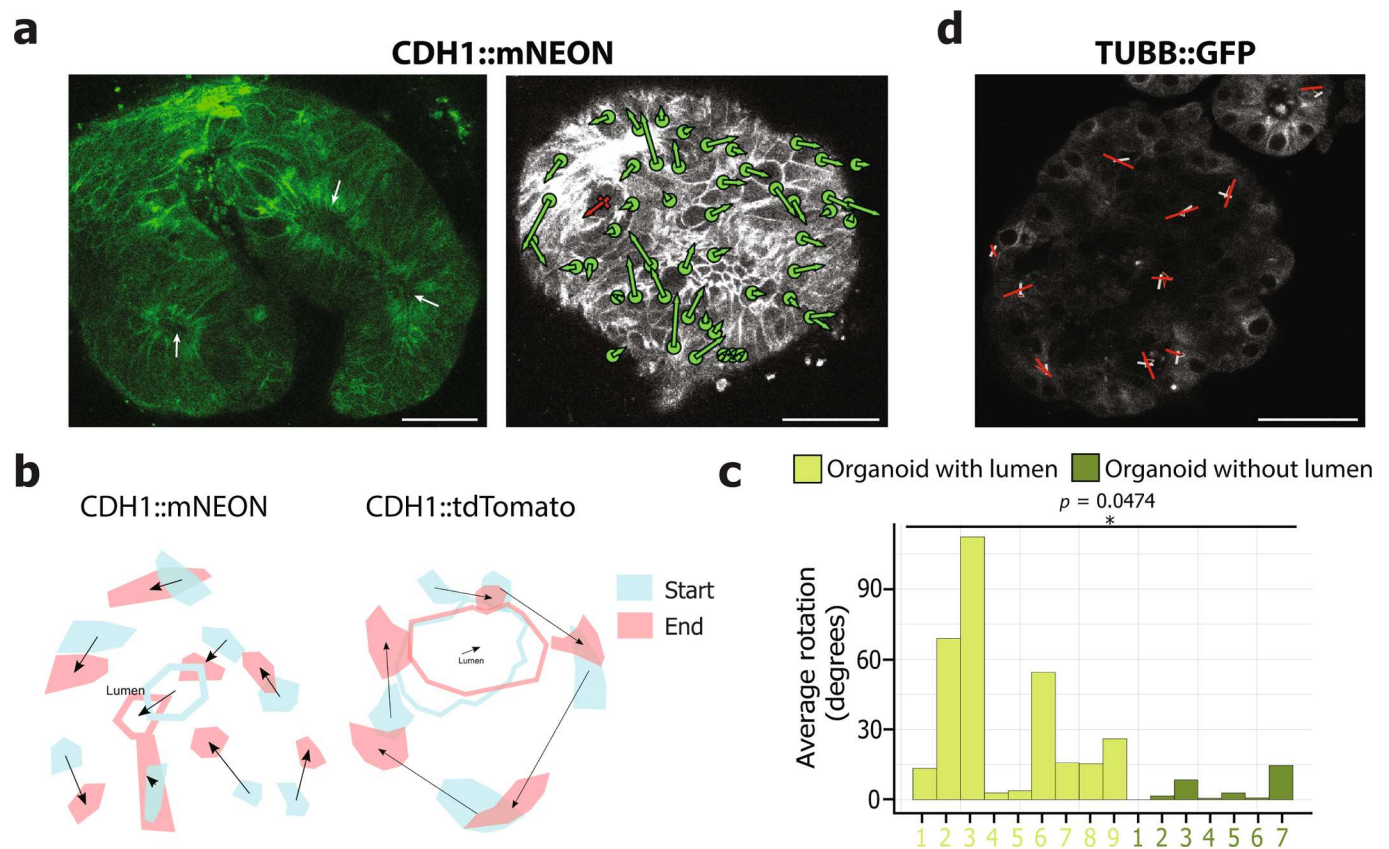


Extended Data Fig. 2 | See next page for caption.

Extended Data Fig. 2 | FACS analysis of knock-in efficiencies mediated by NHEJ or HDR. **a**, Gating strategy and representative plot of how transfected and knocked-in cells were defined based on the negative control (non-transfected cells). **b**, Representative FACS plots of HDR- and NHEJ-mediated knock-in in presence or absence of a dominant negative form of TP53 (DN TP53) when targeting the *TUBB* locus in human hepatocyte organoids. The experiment was repeated three times independently with similar results. **c**, Representative images of electroporated human liver ductal organoids for both HDR- and NHEJ-mediated in-frame knock-in of the respective tag at the *KRT19* locus, showing knocked-in cells overlapping within the transfected cells. The experiment was repeated at least five times independently with similar results. **d**, Bar plot showing fold changes of knock-in efficiency between HDR and NHEJ in presence or absence of a dominant negative form of TP53 (DN TP53) in human liver ductal organoids (targeting the *KRT19* locus) and human hepatocyte organoids (targeting the *TUBB* locus). For liver ductal organoids: n=6 for HDR-DN TP53, n=4 for HDR+DN TP53, n=5 for NHEJ-DN TP53, n=3 for NHEJ+DN TP53, for hepatocyte organoids: all conditions n=3 biological independent experiments. Two-sided unpaired *t*-test performed on the non-normalized data as shown in Fig. 1b-c; **p*<0.05; ***p*<0.01; ****p*<0.001. **e**, Representative brightfield and fluorescent images of HDR- and NHEJ-mediated knocked-in mNEON at the *TUBB* locus in human hepatocyte organoids. Scale bars, c: 200 μ m; e: 20 μ m. Numerical source data for d are provided in Statistical Source Data Extended Data Fig. 2.

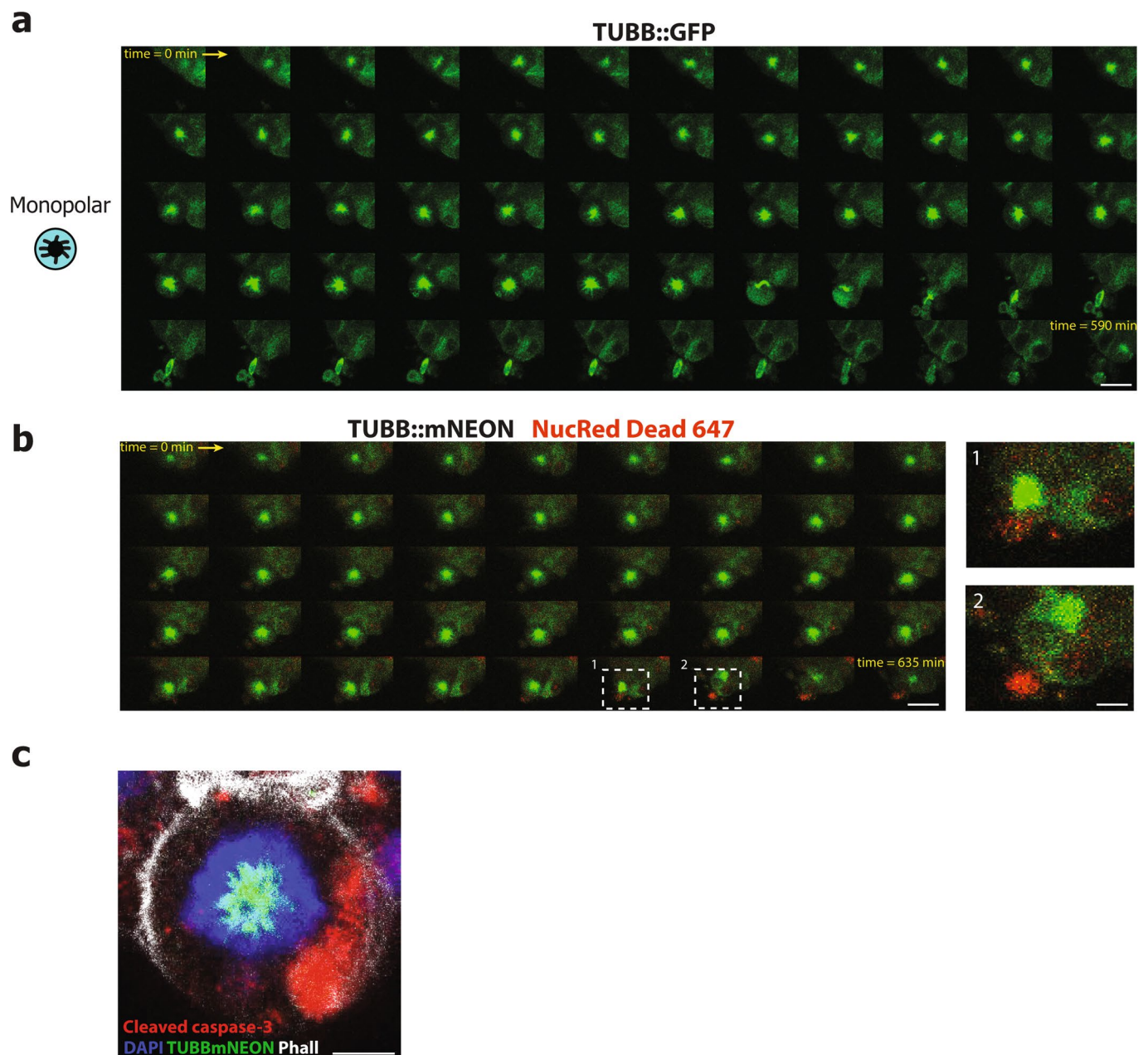
a *KRT18::mNEON***b** *CHGA::mNEON***c** *MUC2::mNEON***d** *AFP::mNEON***e** *TUBB::GFP***f** *CDH1::tdTomato*

Extended Data Fig. 3 | Representative sequencing results of generated human knock-in organoid lines in this study. Sequencing results from clonal organoid lines spanning the insertion site for *KRT18::mNEON* **a**, *CHGA::mNEON* **b**, *MUC2::mNEON* **c**, *AFP::mNEON* **d**, *TUBB::GFP* **e**, *CDH1::tdTomato* **f**. For every targeted locus, sequencing results from 1 of the tagged lines is shown.

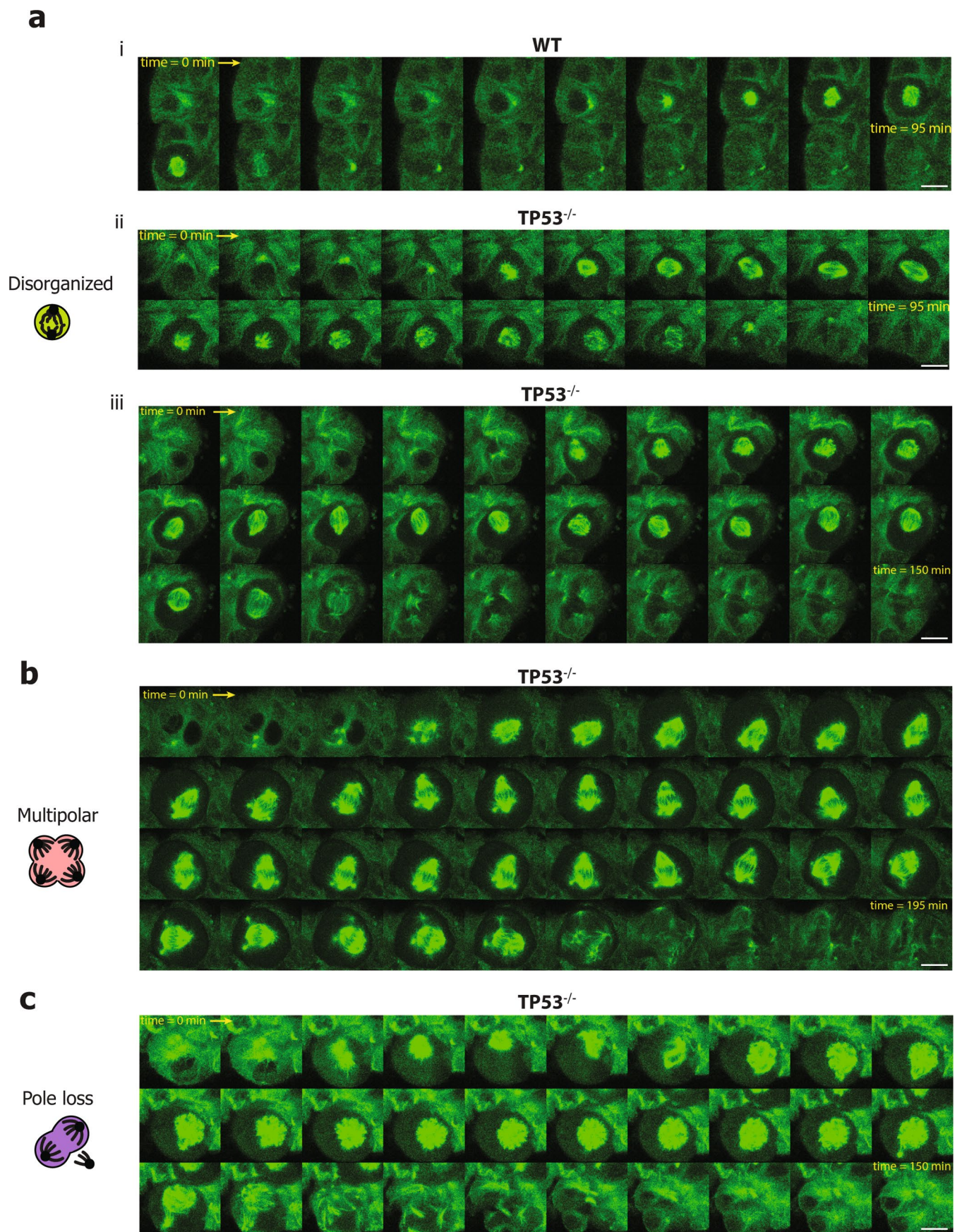


Extended Data Fig. 4 | CDH1-tagged and TUBB-tagged human hepatocyte organoids as a tool for tracing cell movement and mitotic spindle dynamics.

a, Tagging of CDH1 reveals that hepatocytes tend to form rosette structures around lumina (indicated by the white arrows) (left). Representative example of analysis of cell movement in CDH1::mNEON human hepatocyte organoids (right). Individual cell movements were traced based on changes of cell centroid positioning over time. The green dots represent the initial position of the cell centroid and length and orientation of each green arrow represent individual cell centroid movement from begin to end of the experiment. The red line indicates lumen movement. ($t = 9$ hours, 45 min intervals). The experiment was repeated five times independently with similar results. **b**, Representative examples of tracing of cell movement based on changes of cell centroid positioning over time in CDH1::mNEON (left) and CDH1::tdTomato (right) human hepatocyte organoids. Initial and final positioning and cell shape outline are represented in blue and pink, respectively, and cell movements are indicated by arrows. Similarly, the initial and final position of the lumen is outlined and its movement is visualized. Note that hepatocytes tend to rotate around the lumen. **c**, Bar plot showing the average cell rotation for individual organoids with a lumen (light green) or without a lumen (dark green). Note that in organoids in which there is no lumen cells tend to rotate less. as previously mentioned, organoids with a lumen tend to rotate. $n=9$ clonal organoids with a lumen and $n=7$ clonal organoids without a lumen. Two-sided unpaired t -test; $*p < 0.05$. **d**, Example of the determination of mitotic spindle dynamics in TUBB::GFP human hepatocyte organoids. The mitotic spindle orientation was traced over time by marking the initial (gray) and final (red) spindle orientation. The thin line indicates the average position of the spindle poles at every time point between the two. Scale bars, a: left: 75 μ m, right: 100 μ m; d: 100 μ m. Statistics source data are provided in Statistical Source Data Extended Data Fig. 4.

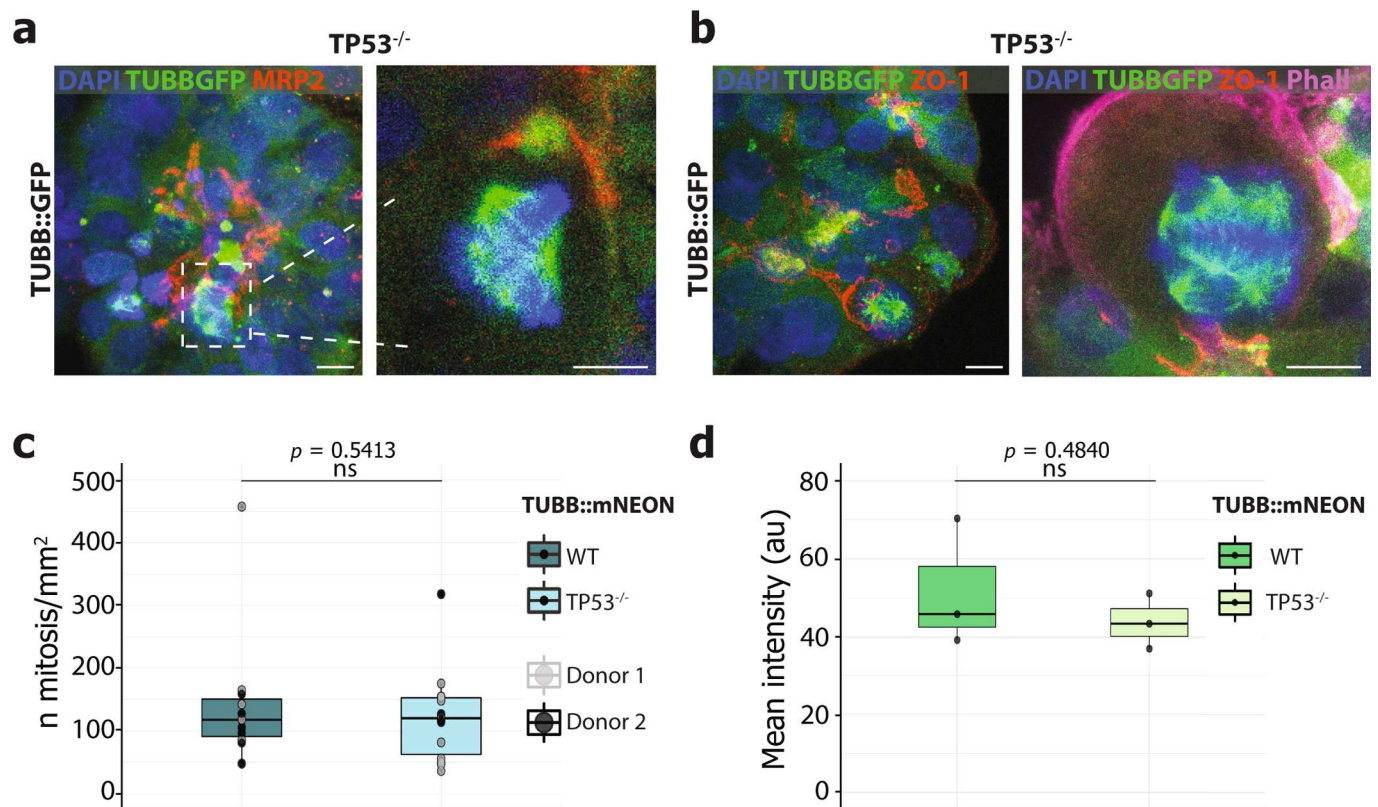


Extended Data Fig. 5 | Characterization of cells with a monopolar spindle in TUBB-tagged human hepatocyte organoids. a, Representative snapshots of a time-lapse experiments showing the formation and fate of monopolar spindles in TUBB::GFP human hepatocyte organoids, resulting in cell bursting. **b**, Representative snapshots of a time-lapse experiments in which organoids were incubated with NucRed Dead 647 confirming that cells with a monopolar spindle die. **c**, Cells with a monopolar spindle stain positive for cleaved caspase-3. All experiments were repeated at least twice independently with similar results. Scale bars, a: 10 μm ; b: left: 10 μm , right: 5 μm ; c: 5 μm .

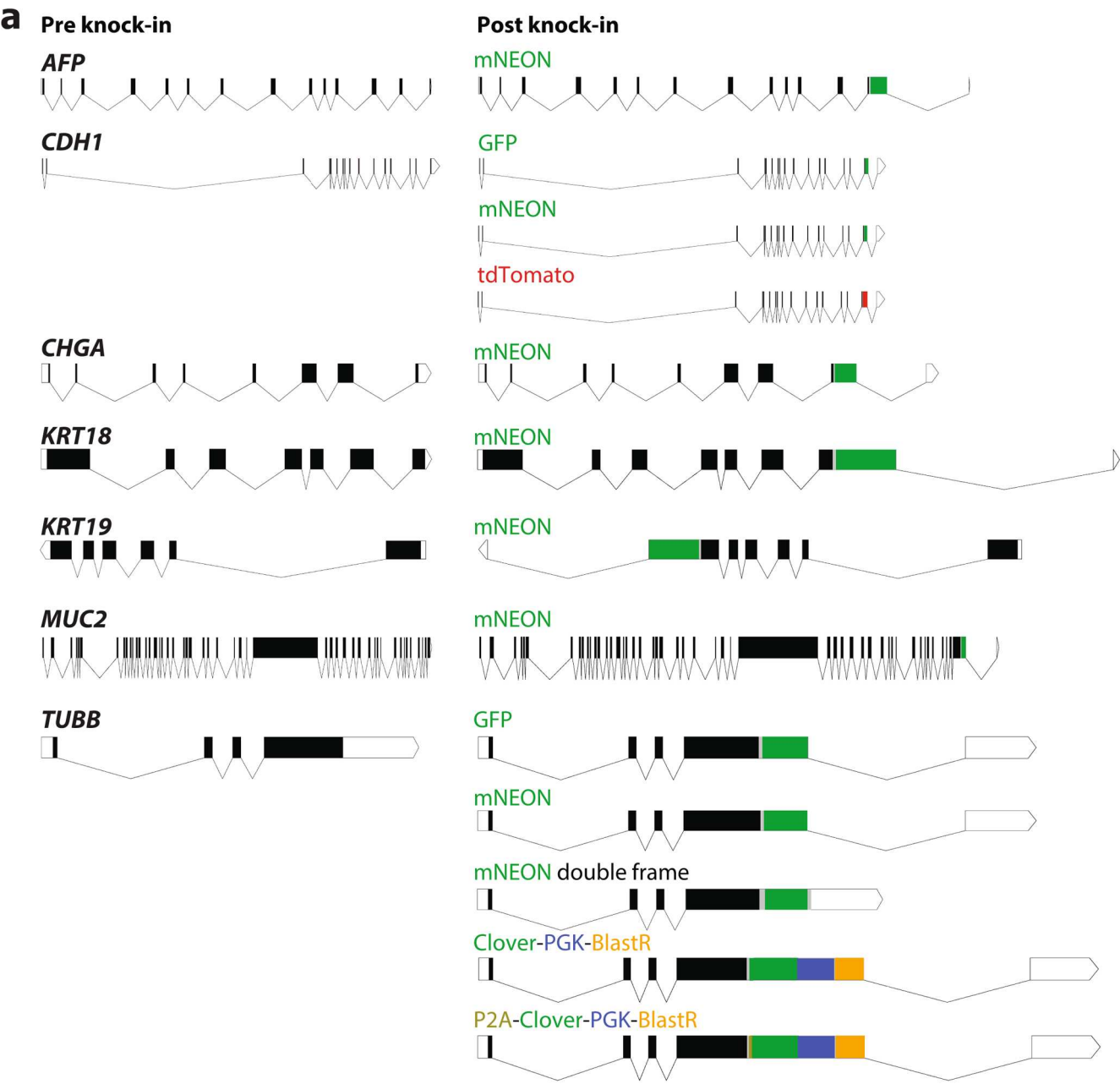


Extended Data Fig. 6 | See next page for caption.

Extended Data Fig. 6 | Types of non-canonical mitotic spindles in WT and TP53^{-/-} human hepatocyte organoids. **a**, Examples of mitotic spindles with disorganized microtubules in a WT (i) and TP53^{-/-} (ii, iii) background. **b**, Loss of TP53 causes frequent formation of multipolar spindles. **c**, Example of a non-canonical mitotic event where a spindle pole is lost in a TP53^{-/-} background. All experiments were repeated at least thirteen times independently with similar results. Scale bars, a-c: 5 μ m.



Extended Data Fig. 7 | Characterization of the impact of TP53 mutation on the phenotype of human hepatocyte organoids. Representative examples of whole-mount (left) and a zoomed-in focal plane (right) staining of TUBB::GFP TP53^{-/-} organoids showing the intactness of the MRP2-marked bile canalicular network **a**, and maintenance of hepatocyte polarity as marked by ZO-1, associated with a cell division with a multipolar spindle **b**. For a-b: experiments were repeated at least twice independently with similar results. **c**, Box-plot showing the amount of mitosis in WT and TP53^{-/-} TUBB-tagged hepatocytes. Each dot (n) represents mitosis quantification in one single organoid. Mitosis in organoids from 2 donors were quantified. Donor 1, WT: n=5; Donor 2, WT: n=6; Donor 1, TP53^{-/-}: n=10; Donor 2, TP53^{-/-}: n=4 biologically independent experiments. **d**, Box-plot showing similar TUBB::mNEON fluorescence intensity between WT and TP53^{-/-} TUBB::mNEON hepatocyte organoids. n=3 biologically independent samples per condition. Box-plot elements shown in c-d are minimum, maximum, centre, 25th percentile, 75th percentile. For c-d: Two-sided unpaired *t*-test. Scale bars, a: left: 10 μ m, inset: 5 μ m; b: left: 10 μ m, right: 5 μ m. Statistics source data for c-d are provided in Statistical Source Data Extended Data Fig. 7.



b

	Hepatocyte	Liver ductal	Small intestine
<i>AFP</i>			
<i>CDH1</i>			
<i>CHGA</i>			
<i>KRT18</i>			
<i>KRT19</i>			
<i>MUC2</i>			
<i>TUBB</i>			

Extended Data Fig. 8 | Schematic overview of all targeted loci in this study. a, Representation of all the genes that have been tagged in this study showing a schematic of the gene pre and post knock-in with all the different tags. Black boxes represent exons, lines represent introns. **b,** Overview of all the genes that have been tagged in the different organoid cultures in this study.